Local neurovascular coupling in the amygdala is responsible for context-dependent emotional adjustment

Jiayu Ruan[1,2,3,4], Xinghua Quan[2,3,4], Huiqi Xie[1,2,3,4], Yiyi Zhang[1,2,3,4], Dongdong Zhang[2,3,4], Wentao Wang[2,3,4], Bingrui Zhao[2,3,4], Danping Lu[2,3,4], Jie-Min Jia[2,3,4*]

Affiliations

1. College of Life Sciences, Zhejiang University, Hangzhou, Zhejiang 310058, China.
2. Westlake Laboratory of Life Sciences and Biomedicine, Hangzhou 310024, China.
3. Key Laboratory of Growth Regulation and Translational Research of Zhejiang Province, School of Life Sciences, Westlake University, Hangzhou 310024, China.
4. Laboratory of Neurovascular Biology, Institute of Basic Medical Sciences, Westlake Institute for Advanced Study, Hangzhou 310024, China.

*Corresponding author. Email: Jie-Min Jia (jiajiemin@westlake.edu.cn)

Abstract

The ability to flexibly regulate emotions in a contextually appropriate manner is essential for individuals to adapt to varying social stresses, and companion inflexibility involves psychiatric diseases. The extent of this flexibility can be quantified by measuring neurovascular coupling (NVC)-based hemodynamics signal through functional brain imaging. However, whether NVC, in turn, plays an active role in emotion regulation remains unknown due to the absence of exclusive strategies for bidirectionally manipulating NVC. By establishing fifteen genetic mouse lines to suppress or enhance NVC, we demonstrated that NVC is an allostatic component that shapes emotion regulation flexibility. With NVC deficits, the same individual mice simultaneously exhibited being overwhelmed (hyper-response) and suppressing emotions (hypo-response), depending on different contexts. Surprisingly, by knocking down vascular mural cell contractile protein, local suppression of NVC within the basal lateral amygdala (BLA), a central emotion regulation hub, induces hyper-response. Mechanistically, such opposite responses were likely attributed to NVC's opposite regulation of BLA's neural activity in a context-dependent manner. Importantly, BLA local neuron-specific chemogenetic antagonization can attenuate hyper-response. More importantly, enhancing NVC alleviated emotional distress induced by acute and chronic restraint stress, highlighting the potential of NVC as a unique therapeutic target that may avoid directly acting on neurons. These findings indicate the active role of NVC in the bidirectional modulation of emotion regulation to fit varying contexts appropriately, emphasizing the necessity of proper NVC for maintaining the homeostasis of advanced brain functions.

Introduction

The flexibility of emotion control, which may be quantitatively measured by functional brain imaging techniques that detect changes in regional cerebral blood flow (rCBF), is essential to survive in varying environmental stresses that produce rapidly changing contextual demands [1,2]. Enhancing flexibility, such as by acceptance and commitment therapy (ACT), benefits psychological and physical health [3-5]. Impaired flexibility is often associated with abnormal neurovascular coupling (NVC) and leads to hypo- or hyper-reactions termed emotion inflexibility, which links diverse psychiatric diseases and even physical well-being [1,4]. For instance, emotional inflexibility, resulting from acute or chronic stresses, is a risk factor for mental health problems such as anxiety, depression, panic disorders, hypervigilance, and agoraphobia [6]. These problems sometimes cause physical health problems such as bowel movement problem like chronic pain and constipation [4,7]. Functional magnetic resonance imaging (fMRI) studies have documented a tight spatiotemporal correlation between rCBF and emotion-mirrored neural activities, belonging to the concept of NVC [8,9]: under the contexts of innate fear or fear-related post-traumatic stress disorder (PTSD), a profound increase in blood-oxygen-level-dependent (BOLD) signal is always observed in the amygdala, a neural hub that has a central role in the regulation of emotions cross species [10-13]. However, whether NVC plays an active role in emotional regulations rather than being a passive measurable parameter remains poorly understood. Therefore, understanding this question may provide a potential therapeutic target that targets vascular cells to regulate emotions and avoids direct actions on neurons, frequently resulting in unwanted severe side effects [14-16].

NVC dysfunction is thought to involve many diseases ranging from neurological to psychological conditions [11,13,17,18]. However, determining the definitive role of NVC in brain

63 functions remained largely experimentally intractable despite NVC being discovered for
64 more than a century [19,20]. Conventional pharmacological interventions to acutely alter
65 NVC, such as broadly active NO synthase (NOS) inhibitors and PGE2 synthase COX2
66 inhibitors to suppress the synthesis of vasodilatory substances, introduce insuperable
67 confounds through initial actions beyond the direct inhibiting NVC and thus lack the cell-
68 type specificity and necessary precision. Available nonspecific genetic interventions by
69 depleting COX2 [21], eNOS [22], nNOS [23], and potassium channel subunit KCNJ8 [24] to
70 suppress NVC chronically. They are also well known to induce severe renal pathology [25],
71 hypertension [26], numerous neural circuit changes [27-29], and vascular arterial smooth
72 muscle cell (aSMC) development deficits [24] that would be unwanted in this context, giving
73 rise to multiple direct confounds for the question explored here. Recently, more specific
74 interventions such as endothelial cell (EC)-specific conditional knockout (cKO) of NMDA
75 receptor core-subunit GluN1 and arteriolar EC-specific (aEC)-Cav1 cKO have been newly
76 developed [22,30]. These may satisfy the question here, but their effects on emotional
77 regulation remain unexplored. In addition, the role of eNMDAR on blood-brain barrier
78 (BBB) integrity should be first evaluated because the damage of BBB integrity in response
79 to stress emerges as a new mechanism to adjust emotional responses [31-33]. On the other
80 hand, explicitly enhancing NVC is a critical, independent aspect of evaluating the question,
81 but to our knowledge, no such genetic models are available. Studying the critical question
82 of how NVC actively regulates emotional states has remained inaccessible, and the effect
83 on behaviour still needs to be discovered.

84 Previously, we have established a synaptic-like transmission mechanism for NVC, a
85 discovery based on the finding of the neuron-smooth muscular junction (NsMJ) [34]. We
86 are now exploring the potential of bidirectional NVC interventions by manipulating cation-

87 and anion-permeable neurotransmitter receptors exclusively at NsMJ, the neurovascular
88 communication interface. We could offer potential interventions to avoid unwanted
89 common side effects of mood stabilizers on neural circuits. These models would enable
90 long-sought functional studies of the physiology of NVC and reveal the active influences
91 on high-order brain functions.
92

93 **Results**

94 ***A variety of genetic models that bidirectional regulate NVC***

95 We first generated fifteen cell-type-specific mouse lines (including corresponding
96 loxp controls) using three different promotors (*SMA-creER*, *Pdgfrβ-creER*, and *Emx1-cre*)
97 across two cell types in the neurovascular unit NVU: mural cells and neurons (Fig. 1a).
98 Their effects on NVC were confirmed through a same examination procedure by
99 measuring the functional hyperemia in the barrel cortex with Laser Speckle Imaging
100 System (LSIS) during the whisker stimulation (Fig.1b). These lines were designed to
101 actively alter NVC using three independent components of NVU: ① blocking NsMJ *(34)*
102 (*SMA-creER:Grin1*$^{f/f}$, *SMA-creER:Grin2d*$^{f/f}$, *SMA-creER:Grin2d*$^{f/f}$*:Grin1*$^{f/f}$, *Pdgfrβ-*
103 *creER:Grin2d*$^{f/f}$, *Pdgfrβ-creER:Grin2d*$^{f/f}$*:Glrb*$^{f/f}$, *Pdgfrβ-creER:Glrb*$^{f/f}$); ② narrowing down
104 traditional study on total COX2 (encoded by gene *Ptsg2*) null mutant *(15)* to neuron-
105 specific (*Emx1-cre:Ptgs2*$^{f/f}$) and aSMC-specific cKO models (*SMA-creER:Ptsg2*$^{f/f}$); ③
106 directly disrupt contractility of mural cells (*Pdgfrβ-creER:Acta2*$^{f/f}$) [35] (Fig. 1a). If these three
107 categories of models truly converged to reveal a similar effect of NVC on emotion-related
108 changes, it would strongly support that is the case.

109 Following our previous work, to examine which subunits assemble with GluN1 to form
110 functional NMDAR in NsMJ [34], we used RT-PCR to detect all NMDAR subunits

expression in sorted parenchymal aSMCs, using cerebellum as a positive control. We found that *Grin2d* (gene name of GluN2D) was the only non-core subunit detected (Fig. 1c, d). RNAscope further confirmed that *Grin2d* puncta appeared in aSMCs of *SMA-creER:Ai14* brain slices (Fig. 1e). The specificity of RNAscope probes was strictly validated in young and adult cerebellum, wherein *Grin2d* is known to show an opposite temporal expression trajectory to *Grin1* [36] (Extended Data Fig. 1a and b). The GluN2D antibody was evaluated by detecting robust signals in the postnatal day 0 (P0) cerebellum, extremely low in neural stem cell promotor (*Nestin-cre*)-driven cKO cerebellum at the same age, and adult cerebellum, where GluN2D is known as barely expressed [37] (Extended Data Fig. 1c). Similar to RNAscope data, GluN2D was found clustered in aSMCs, while it was almost absent in *SMA-creER:Grin2d*$^{f/f}$ cells (Fig. 1f and g). These imaging data were further confirmed by biochemistry elevations *in vitro* (Fig. 1h). Importantly, this absence of GluN2D in *SMA-creER:Grin2d*$^{f/f}$ mice caused no interruptions for neuronal GluN2D expression (Fig. 1i), which also proved the cell-type specificity of *SMA-creER* (Extended Data Fig. 14b,d, and e). Besides, the basal level of contractile proteins, smoothelin and α-SMA, in the *SMA-creER:Grin2d*$^{f/f}$ group did not change, implying basal contraction ability was unaffected (Extended Data Fig. 1d, e). Like GluN1 [34], GluN2D was merely found in aSMCs in peripheral organs, excluding the potential impacts on peripheral systems (Extended Data Fig. 2). Except for specificity inspection, we excluded the possibility of the side effects of tamoxifen and long-term stimulations on whisker stimulation-induced hemodynamic increase (Extended Data Fig. 3). All these examinations indicated that we neither directly altered neural circuits nor caused any functional defects in aSMCs, which is particularly important.

134 Next, we embarked on evaluating NVC for those tamoxifen-induced cKO lines. First
135 of all, singly *SMA-creER:Grin1*$^{f/f}$ and Singly *SMA-creER:Grin2d*$^{f/f}$ produced a similar
136 degree of NVC suppression as that was produced by singly *Pdgfrβ-creER:Grin2d*$^{f/f}$
137 (*Pdgfrβ-creER* specificity inspection analyzed in Extended Data Fig. 14a, c, and e) and
138 doubly *SMA-creER:Grin2d*$^{f/f}$*:Grin1*$^{f/f}$ (Fig. 1j). This again functionally supported GluN2D
139 the only subunit assembled with GluN1 in aSMCs and confirming the role of
140 glutamatergic-NsMJ in NVC [34]. Secondly, *Emx1-cre:Ptgs2*$^{f/f}$ with molecular validations
141 (Extenden data Fig. 4a-c) exhibited robust reduction in NVC (Fig. 1j) to the level of null
142 mutant [21]. Although *Ptgs2* can be detected in aSMC (Extended data Fig. 4d) with the
143 protein level confirmed [38-40] (Extended data Fig. 4e), *SMA-creER:Ptgs2*$^{f/f}$ showed
144 comparable NVC as controls (Fig. 1j), indicating that neurons and aSMC likely used
145 different COX2 signalling pathways to mediate NVC. Thirdly, the reduction of α-SMA, a
146 contractile protein encoded by gene *Acta2*, through *Pdgfrβ-creER:Acta2*$^{f/f}$ in mural cells
147 profoundly damaged NVC (Fig. 1j and k). In brief, compared with previous work, we
148 established different cell-type specifically genetic models that suppressed NVC from three
149 independent components of NVU.

150 Lastly but notably, we successfully established an NVC-upregulation genetic model.
151 Considering that disrupting a cation channel as NMDAR in NsMJ suppresses NVC [34] (Fig.
152 1j), we assumed that disrupting anion channels might enhance NVC. According to past
153 brain SMC transcriptomic studies detected ligand-gating chloride channels, for instance,
154 glycine receptor subunit b (GlyRβ, encoded by gene *Glrb*, Extended data Fig. 4f) showed
155 relative high expression in venular SMCs (vSMCs) [38,39]. We confirmed *Glrb* puncta and
156 protein clusters with more frequency found in vSMCs than aSMCs (Fig. 1l-o). We further
157 identified GlyRβ colocalizing with gephyrin *in vitro* (Fig. 1r), a scaffold protein often

158 segregated in inhibitory postsynaptic sites [41], suggesting that GlyRβ could be clustered
159 on the postjunctional membrane of glycinergic-NsMJ. This speculation was further
160 supported by the finding that frequent direct contact of neural axons onto venular SMCs
161 by both confocal laser scanning microscope (Fig. 1s) and electron microscope (Fig. 1t).
162 We effectively cKO *Glrb* specifically in mural cells using *Pdgfrβ-creER:Glrb*$^{f/f}$ (Fig. 1n, p,
163 and q) and whisker stimulation assay revealed that *Pdgfrβ-creER:Glrb*$^{f/f}$ line enhanced
164 NVC approximately 37.25% higher than averaging from loxp controls (Fig. 1j). These data
165 together supported the viewpoint that glycinergic-NsMJ suppresses NVC at basal
166 homeostasis condition and removal of it leads to enhanced NVC. We predicted that
167 double knockout of *Grin2d* and *Glrb* would neutralize the effects of single cKO on NVC.
168 Indeed, we found no changes in NVC in *Pdgfrb-creER:Grin2d*$^{f/f}$*:Glrb*$^{f/f}$ mice (Fig. 1j), not
169 only providing a stricter control than usual single *Grin2d*$^{f/f}$ or *Glrb*$^{f/f}$ mice but also
170 suggesting that two independent pathways could antagonize with each other.

171 Taking it all together, we have generated genetic models of bidirectional alterations
172 in NVC with cell-type specificity that crossed multiple NVU enterprise components:
173 neurons, mural cells, and NsMJ. With such a variety of genetic tools, we could approach
174 the long-standing question of whether NVC actively regulates emotional responses.

175

176 ***NVC is required to shape the capacity of flexible emotion regulation***

177 Prior to determining whether NVC-deficient mice exhibit an abnormal emotional
178 responses, we first use *SMA-creER:Grin2d*$^{f/f}$ and its control as an example to examine
179 overall physiological features under the home cage context where there would be the
180 minor stress level. All features were comparable between the two lines, including food

181 consumption, water intake, defecation, urination, body weight, blood pressure, and
182 colorectal health inspection (Extended data Fig. 5a-n). Importantly, *SMA-creER:Grin2d*$^{f/f}$
183 and *Pdgfrβ-creER:Grin2d*$^{f/f}$ mice did not show BBB leakage (Extended data Fig. 5o, p).

184 Because defecation and urination behaviours have been documented as emotional
185 index to measure emotional responses in numerous research works regarding anxiety,
186 excitement, or fear-like emotions [42,43], we included them as examination objectives.
187 Surprisingly, only very mild stress, just by switching mice from the home cage to a regular
188 open field box (40*40 cm^2, shortened as OFT_40*40) for 15 min (Fig. 2a), revealed hyper-
189 response in whichever NVC-downregulation models (Fig. 2b-d).

190 Specifically, we examined a total of 228 mice, which comprised eight cKO lines and
191 corresponding controls, leaving out *SMA-creER:Grin2d*$^{f/f}$*:Grin1*$^{f/f}$ (Fig. 2b-c). Notably,
192 qualitative analysis of defecation rate, defined as the fraction of total tested mice that
193 defecated at least once, revealed that all lines with NVC deficiency, regardless of neuron-,
194 aSMC- or mural cell-specific lines, exhibited nearly twice as high as control lines (87.5%-
195 100% vs. 50%-64.29%) (Fig. 2b). And the urination rate was generally consistent
196 (Exyended data Fig. 6). Particularly, in two lines with direct impact on executors of NVC
197 (*Exm1-cre:Ptsg2*$^{f/f}$ and *Pdgfrβ-creER:Acta2*$^{f/f}$), we observed a 100% defecation rate as
198 high as the results from constrictive tube stress assay (Fig. 2a and b), suggesting that the
199 NVC deficit may have made a big splash in emotional regulations.

200 Quantitative analysis consistently revealed that all NVC-deficient lines produced
201 three to four times more total fecal particles than controls (Fig. 2b, c). By contrast, control
202 lines, cKO lines with no NVC deficits (*Pdgfrβ-creER:Grin2d*$^{f/f}$*:Glrb*$^{f/f}$ and *SMA-*
203 *creER:Ptsg2*$^{f/f}$), and NVC enhancement line (*Pdgfrβ-creER:Grin2d*$^{f/f}$) produced around
204 one fecal particle during 15 min (Fig. 2c). Similarly, feces maximum values also indicated

205 the same conclusion (Fig. 2d). These observations suggest that the basal level NVC is a
206 necessarily allosteric component for the brain to avoid generating overwhelmed emotion
207 status under the context of mild stress, where further enhancing NVC above baseline
208 seemed no more benefits (Fig. 2c). By contrast, enhanced NVC (*Pdgfrβ-creER:Glrb*$^{f/f}$)
209 robustly suppressed the defecation amount once the context shifted from OFT to tube
210 stress assay, a much more potent stressor (Fig. 2c). These bidirectional manipulations of
211 NVC suggested that the brain may demand a wide range of NVC capacity to adjust swift
212 emotional responses when switching from context to context.

213 More detailed examinations further consolidated the observations aforementioned.
214 Using *SMA-creER:Grin2d*$^{f/f}$ mice as an example, they responded strongest during the first
215 5 min, showing 12 times more feces and then gradually lesser during the following two 5-
216 min periods, 3.5 folds and 3.0 folds, respectively (Fig. 2e). Besides, there was a
217 profoundly shorter latency, referring to the time needed to produce the first feces, in NVC-
218 deficient mice compared to controls (Fig. 2f). Some cKO individuals immediately
219 defecated after entering the arena, which was never observed in controls. There was no
220 difference in the total running distance and the related time-in-centre parameter for
221 measuring anxiety-like levels of these lines in OFT_40*40 (Extended data Fig. 7).
222 Aforementioned evidence suggested that the defecation-represented emotion was less
223 associated with anxiety under the open-field context.

224 Surprisingly, the size of OFT with gradually decreasing space revealed a neat,
225 negative correlation with the changes in emotion index (defecation), showing gradually
226 increasing fecal particles (Fig. 2g, h). Control mice can distinguish the slight difference in
227 spatial sizes among open-filed areas of 40*40 cm^2 (OFT_40*40), 35*35 cm^2 (OFT_35*35),
228 and 16*38 cm^2 (OFT_16*38) (Fig. 2g, h), reflecting the capacity of modulating the intensity

229 of emotions, a hard-core nature of emotion flexibility to adapt to the demands of a given
230 situation. This behaviour paradigm provided an objective method to explicitly exhibit
231 emotion flexibility, often subjectively measured in human studies by addressing
232 questionnaires [44]. Notably, disrupted flexibility by defective NVC showing abruptly
233 reaching the plateau (Fig. 2h). This data demonstrated that mice with down-regulated
234 NVC lost the capability of emotion flexibility.

235 A summary heatmap including two more genetics-independent manipulations
236 (mentioned below) revealed a qualitative correlation: the basal NVC function was linked
237 to the emotion index (defecation), the higher NVC function was mirrored with the lower
238 emotional index, and the lower NVC function was associated with the higher emotional
239 index (Fig. 2i).

240 In mechanism, to identify functional protein partners of NMDAR within aSMC cytosol,
241 we performed proteomic analysis after co-immunoprecipitation assay using primary
242 aSMCs with overexpression GluN2D. KEGG analysis of the overlapped 75 proteins that
243 were repeatedly identified in three separate independent experiments revealed that the
244 pathway of *vascular smooth muscle cell contraction* was enriched (Extended data Fig.
245 8a). Among proteins in this pathway, caldesmon, a calmodulin-binding protein crucial for
246 SMC contraction and relaxation [45], was further confirmed to interact with GluN2D by
247 Western blotting (Extended data Fig. 8b). Due to the specific expression patterns of
248 caldesmon in mural cells, knocking down caldesmon by cistern magna injection of *Cald*
249 (gene name of caldesmon) siRNA led to NVC downregulation as well as hyper defecation
250 (Extended data Fig. 8c-i). The aforementioned evidence suggested that mechanistically,
251 caldesmon may be the downstream protein of GluN2D in aSMCs for NVC regulation.

252 Besides, previous studies have found that subjecting mice to an eight-week high-fat
253 diet (HFD) led to deficits in NVC and blood-brain barrier (BBB) leakage [17,46,47]. However,
254 whether BBB leakage is the primary cause of NVC deficits is still uncertain. Additionally,
255 if the HFD in humans also results in NVC deficits and emotional inflexibility, an applicable
256 connection between this study and clinical therapy could be established. To clear the
257 relationship between NVC deficits and BBB leakage, we shorted the HFD challenge to
258 four weeks. A robust increase in body weight can be observed from the first week
259 (Extended data Fig. 9a). Importantly, we found that at the end of 4-week HFD, BBB
260 seemed still intact (Extended data Fig. 9b, c) when NVC was damaged (Extended data
261 Fig. d, e) and defecation increased in OFT_40*40 (Fig. 2j), demonstrating NVC deficits
262 and emotional inflexibility occurring earlier than the potential BBB breakage. Interestingly,
263 we found that during the HFD challenge, HFD mice ate less food than control mice
264 (Extended data Fig. 9f) and produced fewer fecal particles during the home cage
265 (Extended data Fig. 9g), further demonstrating that increased emotional index (defecation)
266 is context-dependent and specific to NVC deficits rather than increased food intake. This
267 result raised a stronger temporal association between NVC and emotional changes,
268 providing a potential treatment for high Body Mass Index (BMI) individuals with emotional
269 inflexibility.

270 Given that several reviews have suggested that NVC is one of the critical factors in
271 neurological diseases, especially Alzheimer's disease [48], we compared the accumulation
272 of Amyloid-β plaque in 18-month-old *SMA-creER:Grin1*$^{f/f}$ mice and 5XFAD mice. No
273 apparent plaques were developed in chronic NVC-deficient mice (Extended data Fig. 10).
274 This suggested that a single factor of NVC dysfunction alone cannot induce neurological
275 diseases.

276 In summary, three effects on NVC (upregulated, unchanged, downregulated)
277 observed in these models revealed a negative correlation between the NVC function and
278 the capacity for emotional regulation. This versatility has likely ruled out other
279 contributions of side effects but the indispensable NVC deficit. Taking all results together,
280 we claim that NVC primarily adjusts emotional responses that fit stress levels
281 appropriately.
282
283 ***NVC-deficient mice exhibit decreased fear-like behaviors***
284 We continued to use *SMA-creER:Grin2d*$^{f/f}$ mice as NVC-deficit model to evaluate the
285 universality of the NVC function in emotion regulation beyond the context of switching to
286 a new locomotion environment, such as innate fear of insecure places, innate fear of
287 predators, and social fear of aggressors. Prey C57/B6 mice are believed to feel
288 emotionally and naturally more fearful on white floors and more secure on black floors [49].
289 We separated a chamber with a metal fence into the left with a white floor and the right
290 with a black floor (Fig. 3a). We placed one mouse at a time into the white side. This design
291 allowed the mouse to see through but not be able to cross the fence to get into the darker
292 side so that the travelling time spent and active approaches near the dark side may be
293 used as emotion index of innate fearful-like emotional response to the white side (Fig. 3a).
294 We have named this assessment the "open-field-like test" (OFLT) in this study. Control
295 mice displayed an expected innate fear-like response as evidenced by their longer travel
296 time near the dark side (Fig. 3b-d), longer time to approach the dark side by exhibiting
297 more times of sniffing and climbing the fence (Extended data Fig. 11a, b). Although NVC-
298 deficient mice could cognitively recognize which side was insecure, they exhibited a much
299 lower-level preference to the dark side, implicating lower innate fear-like status while

staying in an insecure place (Fig. 3b-d). Interestingly, hyper-defecation behaviour was again observed under the OFLT context (Extended data Fig. 11c). Given that hyper-defecation may represent higher levels of anxiety, fear, and excitement, what NVC-deficient mice exhibited should belong to hyper-excitement because they had a lower level of fear-like emotion compared to normal mice shown above. Secondly, higher total running distance (Extended data Fig. 11d) observed, a typical hyperactivity phenotype induced by psychostimulants such as morphine [50]. Thus, in a more complex context like the OFLT than OFT, individual mice may simultaneously exhibit decreased innate fear-like emotion and oppositely increased hyper-excitation-like emotion.

Shortened subsiding process after predator-like threats stimulation in NVC-deficient mice

To systemically evaluate the level of innate fear in the NVC-deficient model, mice undergo three threatening paradigms: a video showing an approaching cat, classic looming stimulation imitates predator diving, and virtual reality of eagle hunting (shortened as Cat_{video}, looming, and VR_{eagle}, respectively, Fig. 3e-s).

First, we recorded the behavioural responses of awake, head-fixed mice on a treadmill repeatedly stimulated by Cat_{video} with three trials (Fig. 3e and Supplementary Video. 1). As expected, in response to the first trial, control mice showed the most retreat and tail rattling, typical defensive behaviours when experiencing innate fear (Fig. 3f, g). This demonstrated Cat_{video} was an effective stimulus. Notably, most NVC-deficient mice exhibited no retreat behaviour at all (Fig. 3f). Even among the rest small subset of this group, the intensity of defensive behaviours was also remarkably reduced (Fig. 3i-j).

323 These observations of defensive responses suggest a lower level of innate fear-like status
324 in NVC-deficient mice, supporting the findings from OFLT (Fig. 3a-d).

325 Next, to enhance the observation by the Cat_{video}, we stimulated free-moving instead
326 of head-fixed mice with looming (Fig. 3k). Mice would not receive stimulation until they
327 reached a moving speed of 13-15 cm/s (Fig. 3l) before the stimulation. No differences in
328 locomotion speed can be detected between NVC-deficient mice and their controls before
329 the stimulation (Extended data Fig. 12a). The looming constantly induced consistent
330 subsiding behaviour of both genotypes, showing the reduction of locomotion speed down
331 to 1-2 cm/s shortly after the initiation of stimulation. This observation demonstrated that
332 NVC-deficient mice had normal visual sensation and cognitive understanding of looming
333 threats (Fig. 3l). Notably, the heatmap profile, showing the locomotion speed of all mice
334 for each group, revealed that NVC-deficient mice exhibited shorter subsiding than
335 controls (Fig. 3m). Other behavioural characterizations including shorter latency recovery
336 from subsiding status (Fig. 3n) and lower rearing index (Fig. 3o), which indicates the fear
337 level of mice, observed in NVC-deficient mice. Above evidence, again, reflected a lower
338 innate fear-like status like in Cat_{video} assay (Fig. 3e-j).

339 Lastly, we updated looming system to VR_{eagle} system to threaten mice by delivering
340 an eagle-hunting video played in a ballroom to make more realistic environment (Fig. 3p).
341 As the nonvoluntary change of pupil size serves as an objective measurement for innate
342 fear status [51] and the locomotion speed is an index often used across many studies [52],
343 we recorded these two parameters simultaneously from awake, head-fixed mice placed
344 on a floating ball (Fig. 3p and Supplementary Video. 2). Under basal level, pupil size and
345 locomotion speed between two genotypic were not different (Extended data Fig. 12b and
346 c). Similarly, eagle stimulation was not provided until mice started to move. Eagle

347 stimulation successfully frightened both genotypic mice by showing a similar abrupt rise
348 in pupil size (Extended data Fig. 12d), mirrored by a sudden decrease in locomotion
349 speed (Fig. 3q), again reflecting unchanged cognitive recognition of threats. Based on the
350 aforementioned data, we normalized the locomotion speed at 0s and the pupil size at 3s
351 (Fig. 3q), and we used the intersection point of normalized locomotion speed and
352 normalized pupil size (shown by the arrow in Fig. 3q) as the response index to reflect the
353 subsiding extend. It can be observed that NVC-deficient mice exhibited a lower response
354 index compared with controls (Fig. 3r). Besides, we also examined the subsiding process
355 following imminent fear by measuring the latency of recovering these two parameters (for
356 looming assay used locomotion speed, and for VR_{eagle} assay used pupil size) back to the
357 initial basal level (Fig. 3s) in looming assay and VR_{eagle} assay. To our great surprise, two
358 independent assays revealed a very close fold change in the subsiding duration (Fig. 3s),
359 strongly suggesting that NVC deficiency makes animals recover faster from predator
360 threats. Premature release of the defense state may be fatal because the danger from
361 predators may not have disappeared. Therefore, individuals with shorter fear retention
362 may be preyed upon, and they may have been eliminated earlier in evolution.
363
364 Collectively, all these paradigms were repeatedly applied for three trials (Cat_{video} and
365 looming) or five trials (VR_{eagle}), and most mice show a general adaptation (Extended data
366 Fig. 13). Importantly, independent paradigms (looming and VR_{eagle}) commonly revealed
367 a shared feature, and this significant finding that NVC deficit lowered the level of innate
368 fear-like emotion underscores the importance of our research in understanding fear
369 responses in mice.
370

371 ***NVC-deficient mice are less threatened by a real social aggressor***

372 In addition to virtual stressors, we continued to examine emotion regulation under
373 real threats from cohabitating control or NVC-deficiency mice in the same cage with social
374 aggressor CD1 mice. This cage was partly separated into small and large subregions due
375 to the dented metal top so that the two mice were able to travel between them freely (Fig.
376 3t). Due to naturally fear, the control and NVC-deficient mice tended to avoid CD1 by
377 keeping distance, we predicted that NVC-deficient mice would show less avoidance.
378 Indeed, under the condition that the sniffing recognition process between CD1 and both
379 genotypes of mice was not different (fig.3u), the quantification of the total time when two
380 mice cohabited in the small subregion revealed that the NVC-deficient mice exhibited a
381 longer time (Fig. 3v light color), and so exhibited the total time that recorded which
382 genotype mice took the active entrance into the small region when CD1 had been there
383 (Fig. 3u deep color), indicating that NVC-deficient mice might have a lower intention to
384 avoid aggressive CD1 mice. More strikingly, 98% of control mice fled away from CD1
385 after fights, and so did only 37% of NVC-deficient mice (Fig. 3w left). Consistent with the
386 mice flee rate, we normalized it to total fight events. There were 37 and 19 fights between
387 the 8 controls with CD1 and 10 NVC-deficient mice with CD1, respectively, among which
388 CD1 actively triggered the most fights. NVC-deficient mice exhibited significant smaller
389 percentage of flee rate than controls (Fig. 3w right). These observations strongly
390 supported that even under the context of real stressors, NVC modulated internal
391 emotional status, highlighting that NVC deficit disrupted fear emotion processing.

392

393 ***NVC actively modulates context-dependent emotion flexibility through differently***
394 ***tuning BLA neural activity***

395 Next, we focused on the well-known emotional regulation nucleus, the amygdala, to
396 delineate the mechanism underlying how NVC regulates emotions. We hypothesize that
397 NVC deficiency differentially alters amygdala activity in a context-dependent manner. So,
398 we profiled the expression patterns in the basal lateral amygdala (BLA) of early response
399 gene c-Fos expressions across the aforementioned seven paradigms, shown as
400 heatmaps (Fig. 4a). As expected and consistent with previous reports [53], compared to the
401 home cage, the rest six paradigms all increased c-Fos expressions, but their levels and
402 location patterns varied from context to context (Fig. 4a). We generated a pattern
403 similarity index by a double-blinded data-analysis specialist (see the Method) to conduct
404 an unbiased cluster analysis to see whether the c-Fos expression patterns can represent
405 the corresponding paradigms. Notably, among the seven paradigms, the similarity index
406 between the most similar two paradigms of looming and VR_{eagle} ranked the top one and
407 ranked top two between the home cage and OFT_40*40. This analysis demonstrated that
408 the similarity index was a reliable indicator, and combine with the data in Fig. 3s, this
409 index also suggested that VR_{eagle} is a reliable and updated behavioural assay born out of
410 the looming assay. Thus, we considered that NVC could differentially alter BLA neural
411 activity in a context-dependent way. Apparently, *SMA-creER:Grin2d*$^{f/f}$ mice exhibited
412 disrupted BLA activation patterns across contexts (Fig. 4a bottom panel), which may be
413 the basis of abnormal behaviours.

414 We chose the series of OFT and predator threats as exemplary paradigms for deeper
415 investigations. Within this pool of five contexts, the similarity classification unbiasedly
416 grouped the home cage and two OFT assays into one class while grouped looming and
417 VR_{eagle} into the other class (Fig. 4b). In contrast, this classification messed up in *SMA-*
418 *creER:Grin2d*$^{f/f}$ mice (Fig. 4b). Furthermore, we found that comparing these two genotypic

419 mice, the higher elevation of c-Fos expression in the BLA (hyperactive BLA) under the
420 OFT context, whereas oppositely lower elevation (hypoactive BLA) in the predator context
421 in *SMA-creER:Grin2d*$^{f/f}$ mice compared to controls (Fig. 4c). It is worthy to mention that
422 this observation was consistently repeated by two independent paradigms for each
423 context (Fig. 4c). When plotting the differences in the emotion-index changes and the
424 differences in the c-Fos-expression changes between the two genotypes in one graph,
425 there seemed to be a positive correlation, that is, hyperactive BLA correlating with hyper-
426 excitement under the OFT contexts and hypoactive BLA correlating with hypo-response
427 under the looming and VR_{eagle} contexts (Fig. 4d, see the Methods). This observation of
428 differentially neural regulations by NVC may mechanistic explain how NVC differently
429 modulate emotion regulations in a context-dependent manner.

430 Here remains a question: Is the regulation of emotions by NVC global or specific to
431 a particular nucleus? The NVC manipulations mentioned above were all global. Since we
432 observed context-dependent neural activation in BLA, we expected BLA to be one of the
433 nuclei that could regulate emotions through local NVC manipulation. Therefore, we plan
434 to manipulate NVC locally by injecting *Cald* siRNA to suppress caldesmon expression in
435 BLA. Before we locally injected *Cald* siRNA at BLA, we confirmed that BLA has
436 conservative blood vessels for *Cald* knock-down (Extended data Fig. 14). Caldesmon
437 expression level significantly decreased after acute siRNA interference (Extended data
438 Fig. 15a-c), along with the same defecation increase to global caldesmon interference
439 (Fig. 4e left 4 columns) and global genetically NVC-down regulation mice (Fig. 4f) in
440 OFT_40*40. These results indicate that loss of NVC in BLA is enough to induce emotional
441 regulation. Based on the c-Fos expression pattern in Figure. 4a-c, we predicted that c-
442 Fos in BLA should increase due to the *Cald* knock-down. Indeed, we found that c-Fos

443 expression in BLA of *Cald* siRNA local injection mice exhibited similar both expression
444 increase and expression pattern to globally genetic NVC-deficiency mice (Fig.4a and
445 Extended data Fig. 15d-e), further suggesting that BLA local NVC suppressing through
446 mural cells could induce neural activation increase and hyper-emotional response. Since
447 we confirm BLA is responsible for context-dependent NVC-based emotional adjustment,
448 and neurons in BLA are executors for emotional regulation. Therefore, we chose one
449 assay, OFT_40*40 again, to verify the causal relationship between neural activation and
450 defecation-related emotional regulation by performing BLA local chemogenetic inhibition
451 to antagonise the neural hyper-active in BLA. Before OFT, we determined the
452 effectiveness and specificity of neural inhibition by using 15 min quarantine and tube
453 stress assays. (Extended data Fig. 16a-b). C21, an agonist for chemogenetic receptor
454 (DREAD), could significantly attenuate excess defecation (Extended data Fig. 16b-c). The
455 intraperitoneal injection of saline or C21 causes extra stress. It thus induces a higher
456 basal defecation index (Fig. 4e and Extended data Fig. 16b) than the data shown in earlier
457 OFT_40*40 and Tube stress assays (Fig. 2c). As we expected, we found that suppression
458 of BLA neural activity attenuated the context-induced over-defecation behaviour in both
459 genotypes in OFT_40*40, suggesting that BLA neural activity is required for NVC-
460 dependent emotional regulation (Fig. 4e right 4 columns).
461

462 ***Enhanced NVC mice show emotional resistance to chronic restraint stress***

463 Finally, apart from HFD, we want to find another point to link our study to clinical
464 application. We aimed to determine the role of enhanced NVC in emotion regulation
465 because we found that *Pdgfrβ-creER:Glrb*$^{f/f}$ mice exhibited attenuated abnormal emotion
466 index (defecation) increase in the 15 min tube stress assay, which is a sort of acute

467 restraint stress (ARS, Fig. 2b, c). We hypothesise that loss of Glyβ in mural cells may
468 help to resist stress challenges. To verify it through more dimensions, we continued to
469 embark on 2-hour tube stress every day for 28 consecutive days to achieve the chronic
470 restraint stress (CRS) model (See the Method), which is believed to eventually lead to
471 depression, anxiety and mood-dominant constipation (54-56). After validating the
472 effectiveness of the CRS model (Fig. 5a), we found that control mice and *Pdgfrβ-*
473 *creER:Glrb*$^{f/f}$ mice with CRS exhibited obvious constipation from day 21, showing not only
474 apparent fewer feces production but also dryer, less water-containing feces (Fig. 5b-
475 d). Compared with the data in ARS, the NVC deficiency model cannot exacerbate or
476 ameliorate restraint stress-induced emotional change in response to these two specific
477 contexts. In great contrast, although NVC-enhanced mice (*Pdgfrβ-creER:Glrb*$^{f/f}$) are
478 powerless to maintain body weight during the CRS and even showed significant body
479 weight loss during the CRS (Extended data Fig. 17a), NVC-enhance mice exhibited a
480 robust stress resistance during the CRS, similar to the home cage control group, reflected
481 by showing normal-trend defecation behaviour and fecal quality despite enduring 28 days
482 of torment (Fig. 5b-e). Theses evidence emphasised that NVC may be a new therapeutic
483 target for mood disorders and related gastrointestinal problems. Previous work thought
484 that BBB integrity may be damaged after CRS [54]. To verify it in our model, we inspect the
485 BBB integrity after a 4-week CRS through IgG leakage in parenchyma. No apparent IgG
486 leakage in the cortex and BLA can be detected in all CRS-treated mice, suggesting that
487 the gastrointestinal protective effect during the chronic stress was not due to the
488 secondary impact of BBB leakage but NVC enhancement (Extended data Fig. 17b-e).
489

490 **Discussion**

491 In this study, we developed fifteen genetic models with cell-type-specificity plus two
492 Cre-independent NVC-deficient models (HFD and global/local Cald siRNA), achieving
493 bidirectional regulations of hemodynamic changes during NVC. These models resulted
494 from single or double perturbations of six protein expressions (GluN1, GluN2D, SMA,
495 GlyRβ, COX2, and caldesmon) within mural cells and neurons of NVU (Fig. 1). We then
496 uncovered that NVC actively regulates emotional/affective behaviours in a context-
497 dependent manner through differently modulating the activity of the emotion centre
498 amygdala. Local NVC suppression in BLA could generate similar consequences to global
499 NVC deficits, indicating that BLA is a crucial region for NVC-based emotional regulation.
500 This study implies that active NVC alterations can be critical in causing or ameliorating
501 affective disorders. We propose that NVC in BLA may be a new therapeutic target for
502 treating mood-spectrum disorders.

503 As most gene perturbations in this study were in mural cells, an out layer of
504 vasculature critical for BBB integrity, one may be concerned that there could be side
505 effects independent of NVC playing a more critical role. For instance, BBB leakage and
506 subsequent immune cell infiltration have been documented to have tight associations with
507 affective changes [55]. Through the evens blue/IgG leakage inspection, we have
508 preliminarily ruled out this possibility. Besides, the mural-cell-independent model (neuron-
509 specific *Emx1-cre:Pgst2*$^{f/f}$) consistently yielded the same effects (Fig. 1j and Fig. 2c).
510 Moreover, if it was due to BBB breakage, the *Pdgfrβ-creER:Grin2d*$^{f/f}$*:Glrb*$^{f/f}$ mice, showing
511 no NVC dysfunction, should have exhibited over-defecation behaviours but it did not (Fig.
512 2b-d). BBB leakage is thought to be the primary reason for HFD-induced cognition
513 declines or emotional changes. However, this study provides that NVC dysfunction could
514 be an alternative primary reason because NVC dysfunction and correlated behavioural

515 changes occur earlier than BBB dysfunction (Fig. 2j and Extended data Fig. 9). As for
516 other BBB-irrelevant unknown side effects, it would also be improbable because the only
517 overlapped feature of NVC downregulation among the HFD, knockdown of *Cald* and five
518 other independent lines (*SMA-creER:Grin1*$^{f/f}$, *SMA-creER:Grin2d*$^{f/f}$, *Pdgfrβ-*
519 *creER:Grin2d*$^{f/f}$, *Emx1-cre:Ptgs2*$^{f/f}$, and *Pdgfrβ-creER:Acta2*$^{f/f}$) commonly showed
520 emotional overreactions (Fig. 2i).

521 A growing body of research in neuroscience, neurology, and psychiatry examines
522 how the diverse NVU cells, beyond the canonical roles in regulating CBF, coordinate and
523 modulate brain activity to regulate cognition and emotion over diverse timescales [31,56].
524 This study further consolidates this emerging view by demonstrating that NVC, as the
525 prototypic function of NVU cells, actively regulates emotional flexibility. The space size-
526 dependent defection index indicates that emotional flexibility is quantifiable (Fig. 2g and
527 h). Our genetic models highlight that NVC is essential for shaping such flexibility based
528 on varying contextual demands, which is demonstrated by the finding that NVC
529 dysfunction leads to the loss of such flexibility (Fig. 2h). Furthermore, it suggested that
530 individuals with impaired NVC may exhibit atypical emotional responses to common
531 stressors.

532 The cerebral control over emotional flexibility may involve switching neural circuits to
533 achieve the switch of emotional regulatory strategies. Such a neural switch seems
534 regulated by NVC, as the similarity index analyses between environment shift to virtual
535 threats revealed that the same manipulation of NsMJ-based NVC had opposite effects on
536 different subgroups of BLA neurons (Fig. 4a). This may be attributed to different neural
537 circuits that execute different emotion regulatory strategies with different responses to the
538 same incompatible NVC. This could explain how NVC downregulation potentiated

539 emotional overreaction while conversely shortening subsiding after innate fear. Through
540 the local *Cald* siRNA injection in BLA, we proved the possibility of local NVC suppression,
541 which had never been achieved before. This study first confirmed that BLA neurons are
542 responsible for defecation-related emotional regulation, and the local NVC in BLA may
543 modulate these neurons.

544 To our knowledge, this study, for the first time, developed an NVC upregulated model
545 and demonstrated unprecedented venule-dependent mechanisms underlying NVC.
546 Ultrastructural reconstruction revealed that venular end feet discontinuity was
547 substantially more significant than capillaries and arterioles. In confocal laser scanning
548 imaging, we found that glycinergic-NsMJ located in venules (Fig.1s) and responsible for
549 the NVC upregulation. Previous work mentioned that axon terminals of glycinergic
550 neurons can be observed both in BLA and lateral habenula (LHb) and are involved in
551 depression regulation [57-59]. Notably, under CRS, NVC upregulation ameliorated repeated
552 physical constraints-induced anxiety-like behaviours, while NVC downregulation involved
553 neither exacerbation nor amelioration. This indicates that GlyRβ in mural cells may
554 suppress a defecation-inhibited pathway. Manipulating this pathway would open a new
555 avenue for studying venule-based NVC to regulate emotions.

556 In summary, by leveraging these multiple combinations of different genetic models,
557 we have further broadened the research fields of NVC and emotion regulation. NVC is
558 responsible for balancing emotions in homeostasis. Current mood stabilizers are often
559 accompanied by severe side effects on memory or cognitive functions, a significant
560 reason why patients are reluctant to take them. This study suggests an alternative
561 strategy, targeting NsMJ rather than neurons, to avoid unwanted neural side effects.

562

563 **Methods**

564 ***Animal and animal care***

565 All mouse procedures complied with the Institutional Animal Care and Use
566 Committee (IACUC) guidelines of the School of Life Sciences, Westlake University. All
567 mice were housed in the Westlake University Laboratory Animal Resource Centre with
568 standard animal facilities, which provided a 12-hour light/dark cycle at 25 °C. No more
569 than six mice were fed each cage, and standard chow/water were provided to the mice
570 *ad libitum*. All the genetic information of mice is in Extended data Table 1.

571

572 ***Cell culture***

573 *SMA-creER:Ai47* P0 mice were anesthetized with ice. Surgical tweezers were used
574 to quickly extract the cortex and then transfer it into the 0.25% Trypsin (Thermo Scientific,
575 Cat# 25200072, USA) for 15 min at 37°C. Next, FBS (Gibico, Cat# 10099, USA) was
576 added to block digestion. Then, cells were filted by a 40 μm filter (Falcon, Cat# 352340,
577 CHN). Finally, cells were centrifuged 1,600*g at 4 °C for 5 min and resuspended by
578 SMCM (ScienCell, Cat# 1101, USA) in T25 flasks (Corning, Cat# 430639, USA). When
579 cells reached approximately 80% full of the bottom surface of T25 flasks, tamoxifen (MCE,
580 Cat# HY-13757A, USA) was administrated to cells. Tamoxifen was dissolved in DMSO
581 (Solarbio, Cat# D8371, CHN), and the final concentration of tamoxifen was 5 μM. After a
582 four-day culture, EGFP in cells were expressed. Cells were sorted by MA-900 (Sony,
583 FCCF-MBR, JPN) to obtain $EGFP^+$ cells. Sorted cells were cultured in SMCM for further
584 assay. The purity of cells sorted by the same method was verified in a paper published
585 by our laboratory [60]. For data in Figure. 1q, samples were directly sorted from $Pdgfr\beta^+$
586 cells in brain lysis by using Anti-Pdgfrβ antibody (without cell culture). Then, *Pdgfrβ*$^+$cells

587 were quickly resuspended by Trizol (Sangon Biotec, Cat# B511311-0100, CHN) for RNA
588 extraction. A list of antibodies is in Extended data Table 3. In Figure 1r, Human Umbilical
589 Vein Smooth Muscle Cells (HU-vSMC, Sciencell, Cat# 8020, USA) used for cell culture
590 in Fig. 1r.
591
592 ***RT-PCR***
593 For cultured cells, after obtaining pure sorted $EGFP^+$ cells from the cortex, cells were
594 cultured in 6 cm dishes (Corning, Cat# 430166, USA) with SMCM. After cells reached
595 around 90% density, Trizol was used for the RNA extraction. For brain tissue, after mice
596 were anesthetized with ice, the cortex or cerebellum of the mice was directly taken out,
597 and TRIzol was used for RNA extraction. After extraction, all RNA samples were reverse
598 transcribed to cDNA (50 ng/μl) using HiScript III 1st Strand cDNA Synthesis Kit (Vazyme,
599 Cat# R312-02, CHN). For the Real-Time Polymerase Chain Reaction (RT-PCR), each
600 reaction contained 10 μl of Green Taq Mix (Vazyme, Cat# P131-AA, CHN), 2 μl of cDNA,
601 2 μl of primer pairs (10 μM), and 6 μl of RNAase-free water. Agarose gel electrophoresis
602 used 2 % agarose gel (BIOWESTE, Cat# 111860, ESP) and ran at 220V for 30 min. RT-
603 PCR gel images were obtained from a Tanon imager (Tanon, 1600 Geil imager, CHN). A
604 list of primer pairs is in Extended data Table 2.
605
606 ***RNAscope in situ hybridisation***
607 Horizontal sections (15 μm) of tamoxifen administrated *SMA-creER:Ai14* (for *Grin2d*),
608 *Pdgfrβ-creER:Ai14* (for *Glrb*) and C57/B6 wild-type (for *Grin2d and Grin1* probe inspection)
609 mice brains were obtained by CM1950 (Lecia, Histo-CM1950, DEU). All RNA scope *in*
610 *situ* hybridisation productions were obtained from ACDbio, including RNAscope Multiplex

611 Fluorescent Reagent Kit v2 (ACDbio, Cat# 323100, USA), *Grin2d* probe (ACDbio, Cat#
612 425951-C3, USA), *Grin1* probe (ACDbio, Cat# 431611, USA), and *Glrb* probe (ACDbio,
613 Cat# 1225261-C1, USA). All operations were carried out following the reagent instructions
614 of ACDbio company and published papers [34,61].
615
616 ***Tamoxifen administration for mice***
617 Tamoxifen was dissolved in corn oil (Aladdin, Cat# C116023-500ml, CHN) and orally
618 administered to mice (10 mg/ml, 200 ul per mouse per day). For conditional knockout
619 *Acta2*, tamoxifen was given from P21 to P24. Otherwise, tamoxifen was orally
620 administered to mice from P60 to P63.
621
622 ***Immunofluorescence staining***
623 For Immunofluorescence (IF) staining, after anesthesia with 1% pentobarbital
624 sodium, the mice were perfused with 1X PBS (5 min) and 4% PFA in 1X PBS (5min)
625 through the left ventricle to empty blood and fix tissue. Afterwards, tissue was extracted
626 and fixed by 4% PFA in 1X PBS for 6 hours at 4 °C. For samples like the brain and
627 peripheral organs, samples were sliced into 50 μm (Leica, Histo-VT1200S, DEU). Then,
628 treated samples by 1% Triton X-100 (Diamond, Cat# A110694-0500, CHN) and 0.25%
629 NDS (Jackson Resources, Cat# 017-000-121, USA) in 1X PBS for 60 min at room
630 temperature. After that, samples were rewashed three times by 1X PBS.
631 In the staining process, the primary antibody diluted with 0.1% Triton X-100 in 1X
632 PBS was used to incubate samples overnight at 4 °C. After the incubation, samples were
633 washed with 1X PBS 10 min (3 replicates). The corresponding secondary fluorescence-
634 conjugated antibody diluted with 0.1% Triton X-100 in 1X PBS was used to incubate

635 samples for 120 min at room temperature. After the incubation, samples were washed
636 with 1X PBS 10 min (3 replicates). After that, 1000X diluted DAPI (Beyotime, Cat# C1002,
637 CHN) was used for nucleus staining. Finally, samples were covered by a glass slice with
638 the mounting medium (SouthernBiotech, 0100-01, USA). Zeiss LSM800 (Zeiss, LSM800,
639 DEU) microscopy was used for photography. A list of antibodies is in Extended data Table
640 3.
641
642 ***Western-bolt***
643 For tissue sample collection, samples were ground with RIPA (Thermo Scientific,
644 Cat# 89901, USA) in the tube on ice for 30 min. For cells, after they reached around 90%
645 density, the RIPA was used for protein extraction on ice for 30 min. Protease Inhibitor
646 Cocktail (CWBIO, Cat# CW22008, CHN) was added into RIPA to prevent protein
647 enzymolysis. After that, samples were centrifuged at 12,000*g at 4 °C for 5min, and the
648 supernatant was collected. Concentrations of proteins were measured by Micro BCA
649 Protein Assay kit (CWBIO, Cat# CW2011S, CHN), and all samples were boiled with SDS-
650 PAGE loading buffer (CWBIO, Cat# CW0027S, CHN) for 10 min at 100 °C. 8% SDS-
651 polyacrylamide electrophoresis gels were used for gel running. After 90 min, gels running
652 at 120V (80V for the first 30 min), gels were transferred to 0.45 μm PVDF membranes
653 (Millipore, Cat# IPVH00010, USA) at 400mA for 120 min. After transfer, PVDF
654 membranes were blocked by 5% non-fat milk in 1X TBST buffer for 60 min at room
655 temperature with a mild horizontal shake.
656 After the block, the primary antibody diluted with 5% non-fat milk in 1X TBST buffer
657 was used to incubate the membrane overnight at 4 °C with a mild horizontal shake. After
658 the incubation, the membrane was washed by 1X TBST 10min (3 replicates). The

659 corresponding secondary HRP-conjugated antibody diluted with 5% non-fat milk in 1X
660 TBST buffer was used to incubate the membrane 45 min at room temperature with a mild
661 horizontal shake. After the incubation, the membrane was washed by 1X TBST 10 min (3
662 replicates). ECL kits (Abbkine, Cat# BMU102-CN, CHN) and gel image system (GE, GEL
663 Imaging System AI680RGB v.2.0, USA) were used for exposure photography. A list of
664 antibodies is in Extended data Table 3.
665
666 ***Whisker stimulation***
667 Mice were anesthesia with 1% pentobarbital sodium and open the scalp, then mice
668 stable fixated on the holder. The electro-motor-driven brush stimulated the whisker
669 longitudinally for 1 minute at a frequency of 12 Hz. The principle of laser speckle contrast
670 imaging has been described in the previous paper *(21)*, and the operation referred to in
671 the published paper [34,62,63]. Laser Speckle Image System (RWD, RFSLI ZW/RFSLI III,
672 CHN) was used to record the CBF change in the ROI of the opposite barrel cortex of mice.
673 The recording parameters were 512*512 resolution, 10 FPS, and 2-minute recording. For
674 long-term stimulation assay, data recording was performed on the first and last days of
675 long-term stimulation. The mouse scalp was sutured after the first recording. Subsequent
676 stimulations did not record data until the last stimulation.
677
678 ***Serial block-face scanning electron microscopy image***
679 The specimen was obtained in the same batch as the previously published paper
680 from our laboratory [34]. The details in the “SBF-SEM imaging” section of the methods in
681 that paper. In brief, the ascending venule was identified using X-ray microscopy (Zeiss,
682 XRM, Xradia 520 Versa, DEU) at ×4 and 80 kV magnification. The specimen adhered to

683 an aluminum metal pin using conductive epoxy (Chemtronics, CW2400, USA). Then, it
684 was further precisely trimmed into a block of 600*600*700 μm^3 using a glass knife and a
685 right-angled diamond knife (DiATOME, Trim 90, CHE) after coating with gold-palladium
686 (Leica, EM ACE200, DEU) and a final trim using a 3View ultramicrotome (Gatan, USA).
687 Image acquisition was performed using a BSE detector on a Carl Zeiss Gemini 300
688 scanning electron microscope at 2 kV voltage and approximately $1.8*10^{-3}$ mBar in high-
689 vacuum mode with focus charge compensation. The specimens were sectioned at a 50–
690 75 nm thickness and a cutting speed of 0.1 mm/s.
691
692 ***siRNA cisternal magna/BLA local injection***
693 Cisterna magna injection protocol referred to *Cannula Implantation into the Cisterna*
694 *Magna of Rodents* (https://doi.org/10.3791/57378) and paper published by our laboratory
695 *(34)*. 1nM siRNA was mixed with FITC (10mg/ml, Sigma, FD40S-1G, USA) for injection
696 (20 μl in total). The scalp was opened 10 min after the injection, and the microscope was
697 used to detected the FITC signal (Zeiss, Axio Zoom v16, DEU) in perivascular spaces.
698 Only successfully injected mice remain. Whisker stimulation was performed 48 hours after
699 siRNA injection followed by OFT_40*40. As for BLA local siRNA injection, 150nl of 1nM
700 siRNA was injected in two sides of BLA (AP: -1.55 mm; ML: +/-3.40 mm; DV: -4.00 mm),
701 and OFT_40*40 was performed 48 hours after siRNA injection. Brain slices collection
702 performed after OFT for IF satining. Sequence of siRNA can be found in the Extended
703 data Table 2.
704
705 ***Immunoprecipitation assay***

706 tdTomato^{+} sorted aSMCs from P0 *SMA-creER:Ai14* mice were used for lentivirus
707 infection and further immunoprecipitation (IP) assay. Sorted cells were cultured in 6 cm
708 dishes with SMCM. After cells reach around 90% density, add lentivirus (Lenti-EF1-
709 EGFP-CMV-grin2d-3XFlag-WPRE, virus titer: $2.6*10^{9}$) into the culture and keep for one
710 week to over-express GluN2D. MA-900 sorted out EGFP and tdTomato double-positive
711 cells, which were lentivirus-infected aSMCs. These cells were then cultured in 10 cm
712 dishes. After cells reached around 90% density, cells were collected by RIPA reagent.
713 The Protein G Magnetic beads kit (Epizyme, Cat# YJ002, CHN) was used for the
714 immunoprecipitation assay. GluN2D and IgG control antibodies were mixed with Protein
715 G Magnetic beads to pull down GluN2D and its related protein. Pull-down products were
716 verified by western-bolt and analyzed through mass spectrometry. A list of antibodies is
717 in Extended data Table 3.
718
719 ***Home cage monitor assay***
720 The blood pressure of mice was measured by Kent Noninvasive blood pressure
721 measurement system for animals (Kent/Biopac, USA) before the mice were put into the
722 home cage. Each home cage only contains four mice. In each cycle (three days), 60g of
723 food, 340g of water (including bottle weight), and 100g of padding were provided. Weight
724 of mice, food/water consumption, fecal particles, and urination amount (counted by
725 increased padding weight) were measured by calculate the mean data. Three cycles of
726 monitoring were performed for each home cage. After the assay, mice were fed alone in
727 a clean new cage for 90 min and then used for brain extraction to detect c-Fos expression.
728 The intestine system inspection was performed after three cycles of monitor.
729

730 ***BBB leakage inspection (evens blue)***

731 2% evens blue (Merck, Cat#E2129, USA) in saline was used for orbital injection (4
732 ul/g). After 45 min, the mouse was anesthetized, and the brain was extracted for
733 appearance inspection for BBB leakage using a microscope (Zeiss, Axio Zoom v16, DEU).
734 The brain was weighted and then homogenized using 1 ml of 50% trichloroacetic acid
735 (Merck, Cat#190780, USA). Then, samples were centrifuged at 10,000*g at 4 °C for 20
736 min, supernatants were collected, and absorbance detection at 620 nm was performed.

737

738 **Colorectal inspection**

739 Representative images of colorectal tissue were taken by ENDOQ Colonscopy
740 system. Scoring of the endoscopic images was performed by professional physician in a
741 double-blind manner to ensure unbiased assessment.

742

743 ***Hematoxylin and eosin staining***

744 For hematoxylin and eosin (HE) staining, after anaesthesia with 1% pentobarbital
745 sodium, the mice were perfused with 1X PBS (5 min) and 4% PFA in 1X PBS (5 min)
746 through the left ventricle to empty blood and fix tissue. Afterwards, tissue was extracted
747 and fixed by 4%PFA in 1X PBS for 6 hours at 4 °C. After a paraffin block, tissues were
748 sliced into 8 μm sections and examined following HE staining.

749

750 ***Open field test***

751 The setup of open field test (OFT) referred to published papers [64-67]. Each mouse
752 was placed in the central area of a 40*40 cm, 35*35 cm or 16*38 cm box for the OFT.
753 The camera recording was 15 min. For the chemogenetic manipulation assay, the C21

754 intraperitoneal injection was 45 min before the OFT. After the assay, mice were fed alone
755 in a clean new cage for 90 min and then used for brain extraction to detect c-Fos
756 expression.
757
758 **Quarantine assay**
759 Each mouse was placed in the central area of an empty home cage box for 15 min,
760 60 min, or 24 hrs. Fecal particles was quantified at the end of quarantine assay. For the
761 chemogenetic manipulation, mice were C21 intraperitoneal injected 45 min before the
762 assay, and then each mouse was put into the box for 15 min.
763
764 ***Tube stress assay (ARS & CRS)***
765 A 50ml tube was used to restrain the mice [39,68,69] to perform acute restraint stress
766 (ARS) and chronic restraint stress (CRS). The tube cover and wall will be drilled to ensure
767 normal breathing. For ARS, the mice were restrained in the tube for 15 min, and then the
768 fecal production was measured. For the ARS plus chemogenetic manipulation assay, the
769 C21 intraperitoneal injection was 45 min before the tube stress assay. After the assay,
770 mice were fed alone in a clean new cage for 90 min and then used for brain extraction to
771 detect c-Fos expression. For CRS, the mice were restrained in the tube for 120 min/day,
772 constant for 28 days, and fecal production and Modified Bristol Score (Add “0” to indicate
773 no defecation) was measured at the end of each seven days using 60 min quarantine
774 assays described above.
775
776 ***Open field-like test***

The open field-like test (OFLT) setup referred to a published paper [70]. Each mouse was placed in the central area of the left part of OFLT box. One side of OFLT box has white bottom (mouse put into this side), and black bottom in another side. The camera recording was 20 min. For the analysis, the box was divided into three parts (left area, central area, and right area) to analyze the preference of mice for metal fence (right area close to the metal fence). After the assay, mice were fed alone in a clean new cage for 90 min and then used for brain extraction to detect c-Fos expression.

High fat diet challenge assay

Mice were given high-fat food (SYSE, Cat# PD6001, CHN) for four weeks. The weight of mice and food consumption were measured before the assay, and at the end of each week. The home cage fecal production was measured using the same method mentioned in the “Home cage monitor assay” part. OFT_40*40 assay and whisker stimulation assay were performed after four weeks of HFD challenge.

Cat_{video} stimulation assay

The assay was carried out in a 40*40 cm OFT box. The mouse head was fixed with a fixator and trained to fit the treadmill two weeks before the assay. On the day of the assay, the mice were anesthetized with isoflurane and fixed on the treadmill. After the mouse wakes up, play the video of cat hunting on the iPad Air (Apple. Cat# 3rd generation, USA) in front of the mouse (Supplementary Video 1). The stimulation video played three consecutive times, each stimulation lasting 30 seconds. A camera directly above was used to record the assay.

801 ***Looming assay***

802 The assay was carried out in a 35cm*35cm OFT box. The settings of the assay were
803 based on the published paper [52]. Modifications include:

804 • mice will be put in the OFT box to adapt for 10 min before starting the assay;

805 • we only use a single camera at the top of the box to record;

806 • we stimulate the mice when they move and are not close to the box wall rather
807 than continuously stimulating them.

808 Each mouse performs three trails of stimulations. After the assay, mice were fed
809 alone in a clean new cage for 90 min and then used for brain extraction to detect c-Fos
810 expression.

811

812 ***VR_{eagle} assay***

813 Assay set up referred published paper [51]. The mouse head was fixed with a fixator
814 two weeks before the assay. The mice received daily adaptive training on the VR system
815 one week before the assay. On the day of the assay, the mice were fixed on the VR
816 system and given 5 min of adaptation. Unless stimulated, the screen in front of the mouse
817 will always play the regular landscape video. The stimulation of the eagle lasts for three
818 seconds. The eagle dives down from far to near and plays the voice of the eagle at the
819 beginning of the stimulation. There were five trails of stimulation in total, and the criterion
820 for the first stimulation was that the mice moved for the first time after 5 min of adaptation.
821 The criteria for subsequent stimulation were that the last stimulation ended for at least 2
822 min, and mice resumed movement. The assay ended 2 min after the last stimulation. The
823 pupil changes (Supplementary Video 2) and locomotion speed of mice were recorded at
824 the same time. After the assay, mice were fed alone in a clean new cage for 90 min and

825 then used for brain extraction to detect c-Fos expression. For VR_{eagle} encircle area
826 between curves (ABC) calculations in Extended data Figure. 13b, in brief, we first shift
827 the row data of locomotion speed and pupil size into Z-score, and then we calculate the
828 encircle area by curves of locomotion speed and pupil size from before stimulation to
829 post-stimulation. The larger the encircling area, the more intense the response to the
830 stimulus (because there is a negative correlation between pupil size and locomotion
831 speed when the stimulation reaches its peak).
832
833 ***CD1 social assay***
834 The setup of CD1 fear assay referred to published papers [70-73]. Aggressive CD1 mice
835 never exposed to *Grin2d*$^{f/f}$ or *SMA-creER:Grin2d*$^{f/f}$ mice were used for the assay. Before
836 the assay, simultaneously put a single *Grin2d*$^{f/f}$ or *SMA-creER:Grin2d*$^{f/f}$ mouse and a CD1
837 mouse into a cage. The cage contains new padding and a metal lid on the top. One side
838 of the metal lid is used to place food and water bottles, so the height is lower than the
839 other. A camera was used to record all the behaviours of two mice for 10 min. After the
840 assay, mice were separated again. *Grin2d*$^{f/f}$ or *SMA-creER:Grin2d*$^{f/f}$ mice were fed alone
841 in a clean new cage for 90 min and then used for brain extraction to detect c-Fos
842 expression.
843
844 ***In vivo virus injection***
845 rAAV2/4-Glyt2-EGFP-WPRE-hGHpolyA (5E+12VG/ml) was used for label
846 glycinergic neurons. Two weeks before the assay, bilateral medullary reticular formation
847 injection (500nl on each side, AP: -3.5 mm; ML: +/-0.84 mm; DV: -2.8 mm) was
848 administered [57]. AAV2/5-mCaMKIIa-hM4D(Gi)-EGFP-ER2-WPRE-pA(2.30E+12VG/ml)

849 or AAV2/5-mCaMKIIa-EGFP-ER2-WPRE-pA(2.30E+12VG/ml) were used for the
850 chemogenetical manipulation. Two weeks before the assay, bilateral amygdala injection
851 (150nl on each side, AP: -1.6 mm; ML: +/-3.45 mm; DV: -4.1 mm) was administered [74].
852
853 **Elevated plus-maze test**
854 The setup of elevated plus-maze (EPM) referred to published papers [61,75]. The EPM
855 comprises two open arms (65*5 cm) and two close arms (65*5 cm). Each mouse was
856 placed in the center, facing one of the two open arms, and allowed to explore for 5 min.
857 Time spent in open arms was recorded.
858
859 ***Statistical analysis software and code***
860 All the image processing and analysis of fluorescence intensity used Zeiss Zen Lite (v3.4)
861 and ImageJ (v1.53u). All whisker stimulation original data were measured by RWD LSIS-
862 self software (v5.0). All the original behavioural data for OFT/OFLT/EPM were recorded
863 using Noldus. Data recording and analysis of Looming and VR_{eagle} assay was performed
864 using self-compiled MATLAB codes provided by Bayonne company. All statistical data
865 were processed by Numbers (v12.2). Unless otherwise specified, Student's t test was
866 used for differential analysis on all data that conform to a normal distribution. Non-
867 continuous data that does not conform to a normal distribution, such as fecal particles,
868 signal dots in vessels, and rearing index were analyzed using the Mann-Whitney U test.
869 All figures were made by Prism (v9.4.1) and Adobe Illustrator 2024 (v28.3). CBF peak
870 mean value, heat maps, mass spectrometry data inclusion criteria, and similarity index
871 (based on the Structural Similarity Index, SSIM) were analyzed by self-compiled MATLAB
872 codes. Besides, the KEGG pathways, c-Fos expression pattern classification, and Mann-

873 Whitney U test were analyzed using self-compiled R code. All available code can be found
874 at https://github.com/JialabEleven/Functional_hyperemia_regulates_emotion.
875

876 **References**

877 1 Roelofs, K., Bramson, B. & Toni, I. A neurocognitive theory of flexible emotion control:
878 The role of the lateral frontal pole in emotion regulation. *Ann N Y Acad Sci* **1525**, 28-40
879 (2023). https://doi.org:10.1111/nyas.15003

880 2 Pico-Perez, M., Radua, J., Steward, T., Menchon, J. M. & Soriano-Mas, C. Emotion
881 regulation in mood and anxiety disorders: A meta-analysis of fMRI cognitive reappraisal
882 studies. *Prog Neuropsychopharmacol Biol Psychiatry* **79**, 96-104 (2017).
883 https://doi.org:10.1016/j.pnpbp.2017.06.001

884 3 Gould, R. L. *et al.* Acceptance and commitment therapy for late-life treatment-resistant
885 generalised anxiety disorder: a feasibility study. *Age Ageing* **50**, 1751-1761 (2021).
886 https://doi.org:10.1093/ageing/afab059

887 4 McCracken, L. M. Psychological Flexibility, Chronic Pain, and Health. *Annu Rev Psychol*
888 **75**, 601-624 (2024). https://doi.org:10.1146/annurev-psych-020223-124335

889 5 Hayes, S. C. & Wilson, K. G. Acceptance and commitment therapy: Altering the verbal
890 support for experiential avoidance. *Behav Anal* **17**, 289-303 (1994).
891 https://doi.org:10.1007/BF03392677

892 6 Yao, X. *et al.* Associations between psychological inflexibility and mental health problems
893 during the COVID-19 pandemic: A three-level meta-analytic review. *J Affect Disord* **320**,
894 148-160 (2023). https://doi.org:10.1016/j.jad.2022.09.116

895 7 Yu, Z. *et al.* Altered Resting Brain Functions in Patients With Irritable Bowel Syndrome:
896 A Systematic Review. *Front Hum Neurosci* **16**, 851586 (2022).
897 https://doi.org:10.3389/fnhum.2022.851586
898 8 Hillman, E. M. Coupling mechanism and significance of the BOLD signal: a status report.
899 *Annu Rev Neurosci* **37**, 161-181 (2014). https://doi.org:10.1146/annurev-neuro-071013-
900 014111
901 9 Iadecola, C. Neurovascular regulation in the normal brain and in Alzheimer's disease. *Nat*
902 *Rev Neurosci* **5**, 347-360 (2004). https://doi.org:10.1038/nrn1387
903 10 Whalen, P. J. *et al.* Human amygdala responsivity to masked fearful eye whites. *Science*
904 **306**, 2061 (2004). https://doi.org:10.1126/science.1103617
905 11 Ahmed-Leitao, F., Spies, G., van den Heuvel, L. & Seedat, S. Hippocampal and amygdala
906 volumes in adults with posttraumatic stress disorder secondary to childhood abuse or
907 maltreatment: A systematic review. *Psychiatry Res Neuroimaging* **256**, 33-43 (2016).
908 https://doi.org:10.1016/j.pscychresns.2016.09.008
909 12 Harris, A. P. *et al.* Imaging learned fear circuitry in awake mice using fMRI. *Eur J Neurosci*
910 **42**, 2125-2134 (2015). https://doi.org:10.1111/ejn.12939
911 13 Kamiya, K. & Abe, O. Imaging of Posttraumatic Stress Disorder. *Neuroimaging Clin N*
912 *Am* **30**, 115-123 (2020). https://doi.org:10.1016/j.nic.2019.09.010
913 14 Slattery, P., Frolich, S., Goren, I. & Nusing, R. M. Salt supplementation ameliorates
914 developmental kidney defects in COX-2(-/-) mice. *Am J Physiol Renal Physiol* **312**, F1044-
915 F1055 (2017). https://doi.org:10.1152/ajprenal.00565.2016
916 15 Cryan, J. F., Mombereau, C. & Vassout, A. The tail suspension test as a model for assessing
917 antidepressant activity: review of pharmacological and genetic studies in mice. *Neurosci*
918 *Biobehav Rev* **29**, 571-625 (2005). https://doi.org:10.1016/j.neubiorev.2005.03.009

919 16 Milano, J. *et al.* Antinociceptive action of 4-methyl-5-trifluoromethyl-5-hydroxy-4, 5-
920 dihydro-1H-pyrazole methyl ester in models of inflammatory pain in mice. *Life Sci* **83**,
921 739-746 (2008). https://doi.org:10.1016/j.lfs.2008.09.010
922 17 Huber, G. *et al.* Telmisartan prevents high-fat diet-induced neurovascular impairments and
923 reduces anxiety-like behavior. *J Cereb Blood Flow Metab* **41**, 2356-2369 (2021).
924 https://doi.org:10.1177/0271678X211003497
925 18 Clemm von Hohenberg, C. *et al.* Lateral habenula perturbation reduces default-mode
926 network connectivity in a rat model of depression. *Transl Psychiatry* **8**, 68 (2018).
927 https://doi.org:10.1038/s41398-018-0121-y
928 19 Drew, P. J. Neurovascular coupling: motive unknown. *Trends Neurosci* **45**, 809-819 (2022).
929 https://doi.org:10.1016/j.tins.2022.08.004
930 20 Iadecola, C. The Neurovascular Unit Coming of Age: A Journey through Neurovascular
931 Coupling in Health and Disease. *Neuron* **96**, 17-42 (2017).
932 https://doi.org:10.1016/j.neuron.2017.07.030
933 21 Niwa, K., Araki, E., Morham, S. G., Ross, M. E. & Iadecola, C. Cyclooxygenase-2
934 contributes to functional hyperemia in whisker-barrel cortex. *J Neurosci* **20**, 763-770
935 (2000). https://doi.org:10.1523/JNEUROSCI.20-02-00763.2000
936 22 Chow, B. W. *et al.* Caveolae in CNS arterioles mediate neurovascular coupling. *Nature*
937 **579**, 106-110 (2020). https://doi.org:10.1038/s41586-020-2026-1
938 23 Yang, G., Zhang, Y., Ross, M. E. & Iadecola, C. Attenuation of activity-induced increases
939 in cerebellar blood flow in mice lacking neuronal nitric oxide synthase. *Am J Physiol Heart*
940 *Circ Physiol* **285**, H298-304 (2003). https://doi.org:10.1152/ajpheart.00043.2003

941 24 Ando, K. *et al.* KCNJ8/ABCC9-containing K-ATP channel modulates brain vascular
942 smooth muscle development and neurovascular coupling. *Dev Cell* **57**, 1383-1399 e1387
943 (2022). https://doi.org:10.1016/j.devcel.2022.04.019
944 25 Morham, S. G. *et al.* Prostaglandin synthase 2 gene disruption causes severe renal
945 pathology in the mouse. *Cell* **83**, 473-482 (1995). https://doi.org:10.1016/0092-
946 8674(95)90125-6
947 26 Tsutsui, M., Shimokawa, H., Otsuji, Y. & Yanagihara, N. Pathophysiological relevance of
948 NO signaling in the cardiovascular system: novel insight from mice lacking all NO
949 synthases. *Pharmacol Ther* **128**, 499-508 (2010).
950 https://doi.org:10.1016/j.pharmthera.2010.08.010
951 27 Pigott, B. M. & Garthwaite, J. Nitric Oxide Is Required for L-Type Ca(2+) Channel-
952 Dependent Long-Term Potentiation in the Hippocampus. *Front Synaptic Neurosci* **8**, 17
953 (2016). https://doi.org:10.3389/fnsyn.2016.00017
954 28 Kourosh-Arami, M., Hosseini, N., Mohsenzadegan, M., Komaki, A. & Joghataei, M. T.
955 Neurophysiologic implications of neuronal nitric oxide synthase. *Rev Neurosci* **31**, 617-
956 636 (2020). https://doi.org:10.1515/revneuro-2019-0111
957 29 Yui, K., Kawasaki, Y., Yamada, H. & Ogawa, S. Oxidative Stress and Nitric Oxide in
958 Autism Spectrum Disorder and Other Neuropsychiatric Disorders. *CNS Neurol Disord*
959 *Drug Targets* **15**, 587-596 (2016). https://doi.org:10.2174/1871527315666160413121751
960 30 Hogan-Cann, A. D., Lu, P. & Anderson, C. M. Endothelial NMDA receptors mediate
961 activity-dependent brain hemodynamic responses in mice. *Proc Natl Acad Sci U S A* **116**,
962 10229-10231 (2019). https://doi.org:10.1073/pnas.1902647116

963 31 Dion-Albert, L., Dudek, K. A., Russo, S. J., Campbell, M. & Menard, C. Neurovascular
964 adaptations modulating cognition, mood, and stress responses. *Trends Neurosci* **46**, 276-
965 292 (2023). https://doi.org:10.1016/j.tins.2023.01.005
966 32 Dudek, K. A. *et al.* Neurobiology of resilience in depression: immune and vascular insights
967 from human and animal studies. *Eur J Neurosci* **53**, 183-221 (2021).
968 https://doi.org:10.1111/ejn.14547
969 33 Dion-Albert, L. *et al.* Sex differences in the blood-brain barrier: Implications for mental
970 health. *Front Neuroendocrinol* **65**, 100989 (2022).
971 https://doi.org:10.1016/j.yfrne.2022.100989
972 34 Zhang, D. *et al.* Synaptic-like transmission between neural axons and arteriolar smooth
973 muscle cells drives cerebral neurovascular coupling. *Nat Neurosci* **27**, 232-248 (2024).
974 https://doi.org:10.1038/s41593-023-01515-0
975 35 Arnoldi, R., Hiltbrunner, A., Dugina, V., Tille, J. C. & Chaponnier, C. Smooth muscle
976 actin isoforms: a tug of war between contraction and compliance. *Eur J Cell Biol* **92**, 187-
977 200 (2013). https://doi.org:10.1016/j.ejcb.2013.06.002
978 36 Monyer, H., Burnashev, N., Laurie, D. J., Sakmann, B. & Seeburg, P. H. Developmental
979 and regional expression in the rat brain and functional properties of four NMDA receptors.
980 *Neuron* **12**, 529-540 (1994). https://doi.org:10.1016/0896-6273(94)90210-0
981 37 Laurie, D. J., Bartke, I., Schoepfer, R., Naujoks, K. & Seeburg, P. H. Regional,
982 developmental and interspecies expression of the four NMDAR2 subunits, examined using
983 monoclonal antibodies. *Brain Res Mol Brain Res* **51**, 23-32 (1997).
984 https://doi.org:10.1016/s0169-328x(97)00206-4
985 38 Vanlandewijck, M. *et al.* A molecular atlas of cell types and zonation in the brain
986 vasculature. *Nature* **554**, 475-480 (2018). https://doi.org:10.1038/nature25739

987 39 Yang, A. C. *et al.* A human brain vascular atlas reveals diverse mediators of Alzheimer's
988 risk. *Nature* **603**, 885-892 (2022). https://doi.org:10.1038/s41586-021-04369-3
989 40 Zhang, Y. *et al.* An RNA-sequencing transcriptome and splicing database of glia, neurons,
990 and vascular cells of the cerebral cortex. *J Neurosci* **34**, 11929-11947 (2014).
991 https://doi.org:10.1523/JNEUROSCI.1860-14.2014
992 41 Froehner, S. C. Regulation of ion channel distribution at synapses. *Annu Rev Neurosci* **16**,
993 347-368 (1993). https://doi.org:10.1146/annurev.ne.16.030193.002023
994 42 Sarro, E. C., Sullivan, R. M. & Barr, G. Unpredictable neonatal stress enhances adult
995 anxiety and alters amygdala gene expression related to serotonin and GABA. *Neuroscience*
996 **258**, 147-161 (2014). https://doi.org:10.1016/j.neuroscience.2013.10.064
997 43 Gorard, D. A., Gomborone, J. E., Libby, G. W. & Farthing, M. J. Intestinal transit in anxiety
998 and depression. *Gut* **39**, 551-555 (1996). https://doi.org:10.1136/gut.39.4.551
999 44 Probst, T. *et al.* Development and Initial Validation of a Brief Questionnaire on the Patients'
1000 View of the In-Session Realization of the Six Core Components of Acceptance and
1001 Commitment Therapy. *Clin Psychol Eur* **2**, e3115 (2020).
1002 https://doi.org:10.32872/cpe.v2i3.3115
1003 45 Janovick, J. A., Natarajan, K., Longo, F. & Conn, P. M. Caldesmon: a bifunctional
1004 (calmodulin and actin) binding protein which regulates stimulated gonadotropin release.
1005 *Endocrinology* **129**, 68-74 (1991). https://doi.org:10.1210/endo-129-1-68
1006 46 Chang, H. C. *et al.* Resveratrol attenuates high-fat diet-induced disruption of the blood-
1007 brain barrier and protects brain neurons from apoptotic insults. *J Agric Food Chem* **62**,
1008 3466-3475 (2014). https://doi.org:10.1021/jf403286w

1009 47 Li, W. *et al.* Early effects of high-fat diet on neurovascular function and focal ischemic
1010 brain injury. *Am J Physiol Regul Integr Comp Physiol* **304**, R1001-1008 (2013).
1011 https://doi.org:10.1152/ajpregu.00523.2012
1012 48 Park, L. *et al.* Abeta-induced vascular oxidative stress and attenuation of functional
1013 hyperemia in mouse somatosensory cortex. *J Cereb Blood Flow Metab* **24**, 334-342 (2004).
1014 https://doi.org:10.1097/01.WCB.0000105800.49957.1E
1015 49 Shoji, H. & Miyakawa, T. Effects of test experience, closed-arm wall color, and
1016 illumination level on behavior and plasma corticosterone response in an elevated plus maze
1017 in male C57BL/6J mice: a challenge against conventional interpretation of the test. *Mol*
1018 *Brain* **14**, 34 (2021). https://doi.org:10.1186/s13041-020-00721-2
1019 50 Mickley, G. A., Stevens, K. E., White, G. A. & Gibbs, G. L. Endogenous opiates mediate
1020 radiogenic behavioral change. *Science* **220**, 1185-1187 (1983).
1021 https://doi.org:10.1126/science.6857244
1022 51 Wang, L., Chen, I. Z. & Lin, D. Collateral pathways from the ventromedial hypothalamus
1023 mediate defensive behaviors. *Neuron* **85**, 1344-1358 (2015).
1024 https://doi.org:10.1016/j.neuron.2014.12.025
1025 52 Shang, C. *et al.* Divergent midbrain circuits orchestrate escape and freezing responses to
1026 looming stimuli in mice. *Nat Commun* **9**, 1232 (2018). https://doi.org:10.1038/s41467-018-
1027 03580-7
1028 53 Hale, M. W. *et al.* Exposure to an open-field arena increases c-Fos expression in a
1029 distributed anxiety-related system projecting to the basolateral amygdaloid complex.
1030 *Neuroscience* **155**, 659-672 (2008). https://doi.org:10.1016/j.neuroscience.2008.05.054

1031 54 Lee, S. *et al.* Real-time in vivo two-photon imaging study reveals decreased cerebro-
1032 vascular volume and increased blood-brain barrier permeability in chronically stressed
1033 mice. *Sci Rep* **8**, 13064 (2018). https://doi.org:10.1038/s41598-018-30875-y
1034 55 Kolhe, J. V., Chhipa, A. S., Butani, S., Chavda, V. & Patel, S. S. PCOS and Depression:
1035 Common Links and Potential Targets. *Reprod Sci* **29**, 3106-3123 (2022).
1036 https://doi.org:10.1007/s43032-021-00765-2
1037 56 Taler, M. *et al.* Regulatory effect of lithium on hippocampal blood-brain barrier integrity
1038 in a rat model of depressive-like behavior. *Bipolar Disord* **23**, 55-65 (2021).
1039 https://doi.org:10.1111/bdi.12962
1040 57 Zeilhofer, H. U. *et al.* Glycinergic neurons expressing enhanced green fluorescent protein
1041 in bacterial artificial chromosome transgenic mice. *J Comp Neurol* **482**, 123-141 (2005).
1042 https://doi.org:10.1002/cne.20349
1043 58 Rampon, C., Luppi, P. H., Fort, P., Peyron, C. & Jouvet, M. Distribution of glycine-
1044 immunoreactive cell bodies and fibers in the rat brain. *Neuroscience* **75**, 737-755 (1996).
1045 https://doi.org:10.1016/0306-4522(96)00278-3
1046 59 Cui, Y. *et al.* Astroglial Kir4.1 in the lateral habenula drives neuronal bursts in depression.
1047 *Nature* **554**, 323-327 (2018). https://doi.org:10.1038/nature25752
1048 60 Li, X. *et al.* Proteins secreted by brain arteriolar smooth muscle cells are instructive for
1049 neural development. *Mol Brain* **15**, 97 (2022). https://doi.org:10.1186/s13041-022-00983-
1050 y
1051 61 Yu, X. D. *et al.* Distinct serotonergic pathways to the amygdala underlie separate
1052 behavioral features of anxiety. *Nat Neurosci* **25**, 1651-1663 (2022).
1053 https://doi.org:10.1038/s41593-022-01200-8

1054 62 Boas, D. A. & Dunn, A. K. Laser speckle contrast imaging in biomedical optics. *J Biomed*
1055 *Opt* **15**, 011109 (2010). https://doi.org:10.1117/1.3285504
1056 63 Jin, Y. *et al.* Precise control of embolic stroke with magnetized red blood cells in mice.
1057 *Commun Biol* **5**, 136 (2022). https://doi.org:10.1038/s42003-022-03082-9
1058 64 Liu, C. Y. *et al.* Saikosaponin D exerts antidepressant effect by regulating Homer1-
1059 mGluR5 and mTOR signaling in a rat model of chronic unpredictable mild stress. *Chin*
1060 *Med* **17**, 60 (2022). https://doi.org:10.1186/s13020-022-00621-8
1061 65 Guo, Z., Li, S., Wu, J., Zhu, X. & Zhang, Y. Maternal Deprivation Increased Vulnerability
1062 to Depression in Adult Rats Through DRD2 Promoter Methylation in the Ventral
1063 Tegmental Area. *Front Psychiatry* **13**, 827667 (2022).
1064 https://doi.org:10.3389/fpsyt.2022.827667
1065 66 Kim, S., Hong, K. B., Kim, S., Suh, H. J. & Jo, K. Creatine and taurine mixtures alleviate
1066 depressive-like behaviour in Drosophila melanogaster and mice via regulating Akt and
1067 ERK/BDNF pathways. *Sci Rep* **10**, 11370 (2020). https://doi.org:10.1038/s41598-020-
1068 68424-1
1069 67 Lapmanee, S., Charoenphandhu, J., Teerapornpuntakit, J., Krishnamra, N. &
1070 Charoenphandhu, N. Agomelatine, venlafaxine, and running exercise effectively prevent
1071 anxiety- and depression-like behaviors and memory impairment in restraint stressed rats.
1072 *PLoS One* **12**, e0187671 (2017). https://doi.org:10.1371/journal.pone.0187671
1073 68 Oh, Y. S. *et al.* SMARCA3, a chromatin-remodeling factor, is required for p11-dependent
1074 antidepressant action. *Cell* **152**, 831-843 (2013). https://doi.org:10.1016/j.cell.2013.01.014
1075 69 Seo, J. S. *et al.* NADPH oxidase mediates depressive behavior induced by chronic stress
1076 in mice. *J Neurosci* **32**, 9690-9699 (2012). https://doi.org:10.1523/JNEUROSCI.0794-
1077 12.2012

1078 70 Arakawa, H., Arakawa, K., Blanchard, D. C. & Blanchard, R. J. Scent marking behavior
1079 in male C57BL/6J mice: sexual and developmental determination. *Behav Brain Res* **182**,
1080 73-79 (2007). https://doi.org:10.1016/j.bbr.2007.05.007
1081 71 Borelli, K. G. *et al.* Neural correlates of scent marking behavior in C57BL/6J mice:
1082 detection and recognition of a social stimulus. *Neuroscience* **162**, 914-923 (2009).
1083 https://doi.org:10.1016/j.neuroscience.2009.05.047
1084 72 Arakawa, H., Arakawa, K., Blanchard, D. C. & Blanchard, R. J. A new test paradigm for
1085 social recognition evidenced by urinary scent marking behavior in C57BL/6J mice. *Behav*
1086 *Brain Res* **190**, 97-104 (2008). https://doi.org:10.1016/j.bbr.2008.02.009
1087 73 McQuaid, R. J., Audet, M. C. & Anisman, H. Environmental enrichment in male CD-1
1088 mice promotes aggressive behaviors and elevated corticosterone and brain norepinephrine
1089 activity in response to a mild stressor. *Stress* **15**, 354-360 (2012).
1090 https://doi.org:10.3109/10253890.2011.623249
1091 74 Khalil, V. *et al.* Subcortico-amygdala pathway processes innate and learned threats. *Elife*
1092 **12** (2023). https://doi.org:10.7554/eLife.85459
1093 75 Liu, J. *et al.* Glutamatergic Neurons in the Amygdala Are Involved in Paclitaxel-Induced
1094 Pain and Anxiety. *Front Psychiatry* **13**, 869544 (2022).
1095 https://doi.org:10.3389/fpsyt.2022.869544
1096

1097 **Acknowledgments**

1098 We thank Y. T. and X. H. for sharing *Nestin-cre* and *Emx1-cre* mice. We thank Y. Z.
1099 for sharing psychological knowledge to facilitate our understanding of data. We thank Y.
1100 N. for KEGG map drawing. We thank Westlake University Laboratory Animal Resource
1101 Centre for guiding behaviour assays. We thank the Microscopy Core Facility of Westlake

University for imaging guidance. We thank the Mass Spectrometry & Metabolomics Core Facility (MSMCF) of Westlake University for mass data collection. We thank the Flow Cytometry Core Facility (FCCF) for cell sorting assistance.

Author contributions

J.-M.J. conceived the project, designed the experiments, and supervised this study. J.R. did primary experiments, obtained and organized majority original data, and wrote the manuscript draft. X.Q. participated in behavioural assay design and operations, siRNA cisternal magna injection, gut health inspection assay, BBB integrity inspection, cluster analysis of similarity index, and wrote Mann-Whitney U test R code. H.X. participated in the looming assay and VReagle assay, as well as in blood pressure measurement and long-term whisker stimulation. Y.Z.wrote the main MATLAB code. D.Z. provided primer pairs of Grin1 and critical suggestions. W.W. contributed to the writing of MATLAB code with Y.Z.. B.Z. participated in the genotyping of mice and cell sorting. D.L. helped the mouse brain section.

Competing interests

The authors declare that they have no competing interests.

Materials & Correspondence

Should be addressed to J.-M.J. Necessary data needed to evaluate the conclusions in the paper are present in the paper and/or the Extended data. More information please contact the corresponding author.

Funding

J.-M.J. acknowledges the support from Westlake Laboratory of Life Sciences and Biomedicine (project No. 202309002), Westlake University startup funding, the Westlake Education Foundation, Zhejiang, Key R&D Program of Zhejiang (2024SSYS0031), and the National Natural Science Foundation of China (project No. 32170961).

Figures and figure legends

Figure 1

Ruan et al.

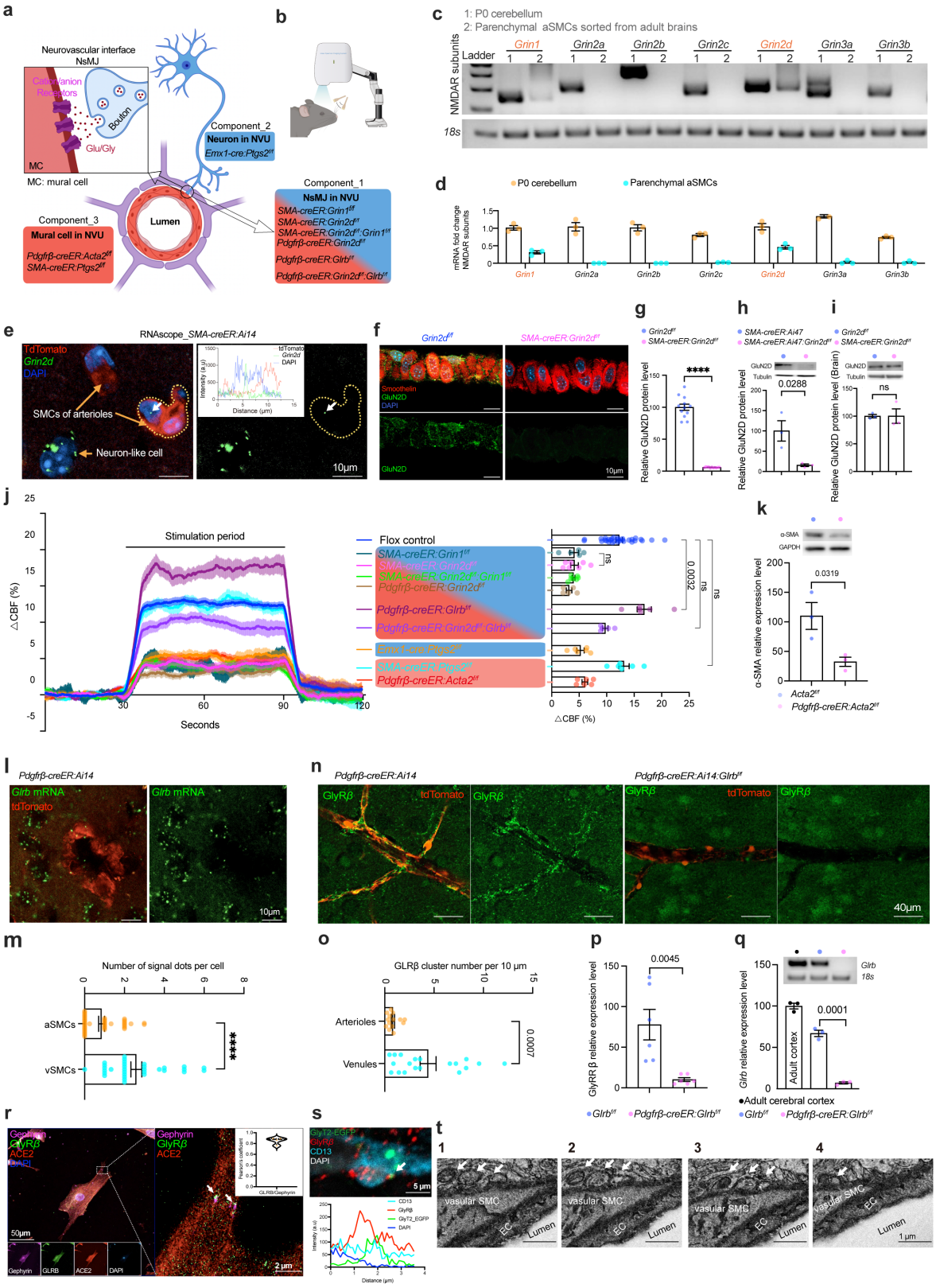

1134 **Fig.1 Bidirectional NVC genetic models. a,** The schematic diagram of three
1135 components in NVU targeted by genetic manipulations. MC: mural cell. **b,** The schematic
1136 diagram of LSIS recording during the whisker stimulation. **c,** mRNA expression levels of
1137 all subunits of NMDARs in primary aSMCs. **d,** The quantification for Figure. 1c. 3
1138 biological replications. **e,** RNAscope detection of *Grin2d* transcripts in brain slices of *SMA-*
1139 *creER:Ai14* mice. The white arrow pointed to *Grin2d* mRNA, plotted in the inserted
1140 histogram. **f,** The immunofluorescence staining of GluN2D in the arterioles of *Grin2d*$^{f/f}$
1141 and *SMA-creER:Grin2d*$^{f/f}$ mice. **g,** The quantification for Figure. 1f. n=12 SMCs for
1142 *Grin2d*$^{f/f}$, and n=11 SMCs for *SMA-creER:Grin2d*$^{f/f}$. ****P<0.0001. **h,** The expression of
1143 GluN2D in the sorted aSMCs from *SMA-creER:Ai47* and *SMA-creER:Ai47:Grin2d*$^{f/f}$ mice.
1144 3 biological replications. **i,** The expression of GluN2D in the cerebral cortex of *Grin2d*$^{f/f}$
1145 and *SMA-creER:Grin2d*$^{f/f}$ mice. 3 biological duplications. **j,** CBF changes in barrel cortex
1146 upon whisker stimulation. The mean of CBF changes from individual mice plotted in the
1147 right panel (n=30 mice for flox control, n=5 mice for *SMA-creER:Grin1*$^{f/f}$, n=7 mice for
1148 *SMA-creER:Grin2d*$^{f/f}$, n=7 mice for *SMA-creER:Grin2d*$^{f/f}$*:Grin1*$^{f/f}$, n=5 mice for *Pdgfrβ-*
1149 *creER:Grin2d*$^{f/f}$, n=6 mice for *Pdgfrβ-creER:Glrb*$^{f/f}$, n=5 mice for *Pdgfrβ-*
1150 *creER:Grin2d*$^{f/f}$*:Glrb*$^{f/f}$. n=6 mice for *Emx1-cre:Ptgs2*$^{f/f}$. n=6 mice for *SMA-creER:Ptgs2*$^{f/f}$,
1151 and n=6 mice for *Pdgfrβ-creER:Acta2*$^{f/f}$). **k,** The expression of α-SMA in the cerebral
1152 cortex of *Acta2*$^{f/f}$ and *Pdgfrβ-creER:Acta2*$^{f/f}$ mice. 3 biological replications. **l,** RNAscope
1153 detection of *Glrb* transcripts in brain slices of *Pdgfrβ-creER:Ai14* mice. **m,** The
1154 quantification of mRNA signal dots in aSMCs and vSMCs for Figure. 1m (n=41 cells for
1155 aSMCs, and n=32 cells for vSMCs). ****P<0.0001. **n,** The expression of GlyR*β* in brain
1156 slices of *Pdgfrβ-creER:Ai14* and *Pdgfrβ-creER:Glrb*$^{f/f}$*:Ai14* mice. **o,** The statistical data of
1157 GlyR*β* clusters in aSMCs and vSMCs of *Pdgfrβ-creER:Ai14* mice in Figure. 1n (n=14

1158 arterioles, and n=19 venules). **p,** The quantification of GlyRβ immunosignal intensity for
1159 Figure. 1n (n=6 mice for each group). **q,** Semi-quantitative analysis of *Glrb* mRNA by RT-
1160 PCR for the sorted PDGFRβ^{+} cells in the cerebral cortex of *Glrb*$^{f/f}$ and *Pdgfrβ-creER:Glrb*$^{f/f}$
1161 mice. 3 biological replications. **r,** Co-immunostaining of GlyR*β* and Gephyrin in HUvSMC.
1162 The white arrow marked their colocalizations. Right up panel is the statistical co-
1163 localization analysis (n=4 cells). **s,** The diagram is glycinergic NsMJ in a venule. The
1164 bottom profile analysis ROI is indicated by the white arrow in the top image. **t,** Serial SEM
1165 sections of the ascending venule in mouse cerebral cortex. The white arrows point to
1166 presynaptic boutons of NsMJ in venules. Data are presents as mean ± SEM.
1167

Figure 2

Ruan et al.

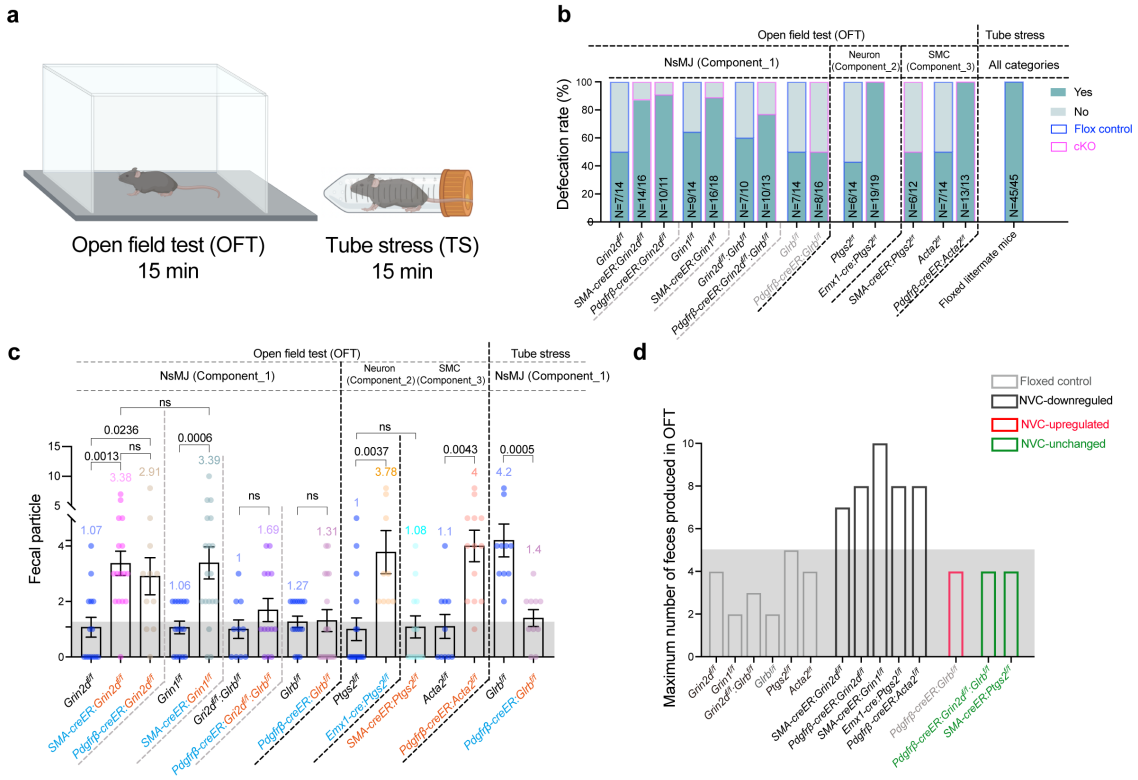

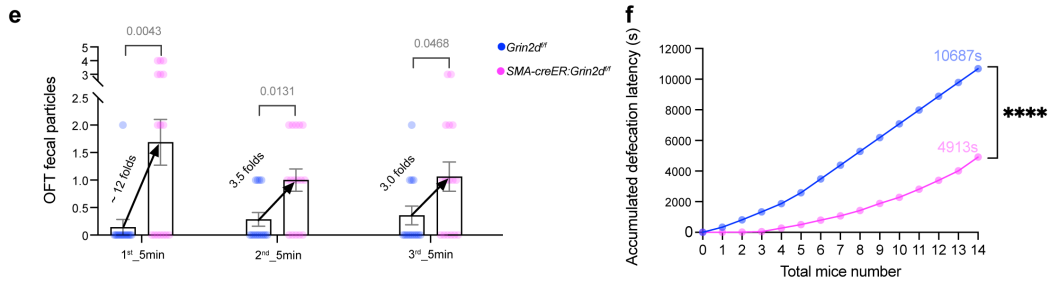

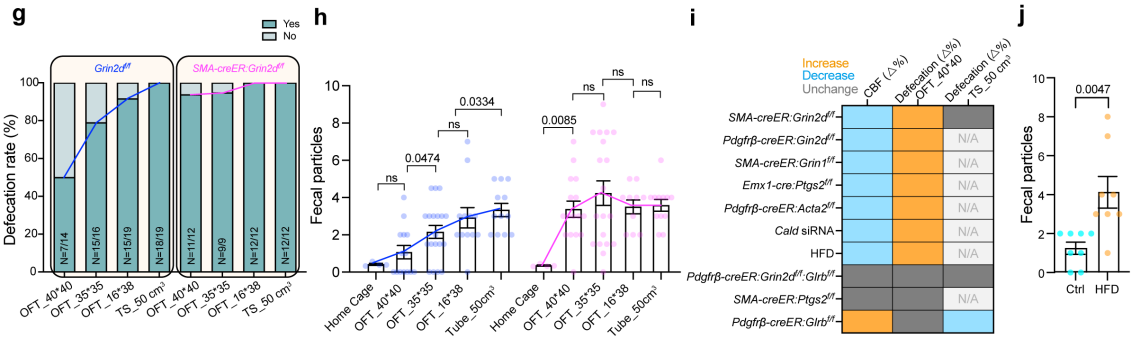

1170 **Fig. 2 NVC is required to actively modulate the capacity of flexible emotion**
1171 **regulation. a,** The schematic diagram of the OFT and Tube stress. **b,** The defecation
1172 rates of each mouse line subjected to the assay of OFT_40*40 and that of all summed
1173 six loxp control lines subjected to tube stress. **c,** The total number of fecal particles
1174 produced by each line within a 15-minute period of OFT_40*40 and that produced by the
1175 *Glrb* gene-modified lines within the same period of tube stress. The gray area indicates
1176 the mean fecal production in all loxp control groups. **d,** The maximum feces number
1177 produced by each line subjected to the OFT_40*40 assay. Raw data generating b-d
1178 panels shared the same bunch of mice. Mouse numbers (N) used for each line were listed
1179 in Figure. 2b. **e,** The feces production within every 5 min during the 15-minute OFT_40*40
1180 assay (n = 14 mice for *Grin2d*$^{f/f}$, and n=16 mice for SMA-creER:*Grin2d*$^{f/f}$). The gray area
1181 indicates the maximum fecal production in all loxp control groups. **f,** The cumulative
1182 defecation latency summarized from fourteen mice for each genotype subjected to the
1183 OFT_40*40 assay (n=14 mice for each group). ****P<0.0001. **g,** The defecation rates for
1184 the OFTs of 40*40 cm^2, 35*35 cm^2, 16*38 cm^2, and the 50 cm^3 tube assay. **h,** The total
1185 number of fecal particles produced in Figure. 2g. The raw data generating in figure. 2c
1186 (*Grin2d*$^{f/f}$ and *SMA-creER:Grin2d*$^{f/f}$), 2g and 2h shared the same bunch of mice, and the
1187 total mouse number (N) used is listed in Figure. 2g. **i,** The negative correlative relationship
1188 between NVC changes and defecation activity recorded in the assays of OFT_40*40 and
1189 tube stress. **j,** The fecal production in OFT_40*40 of normal mice with or without prior
1190 HFD challenge (n=8 for each group). Data are presents as mean ± SEM.

Figure 3

Ruan et al.

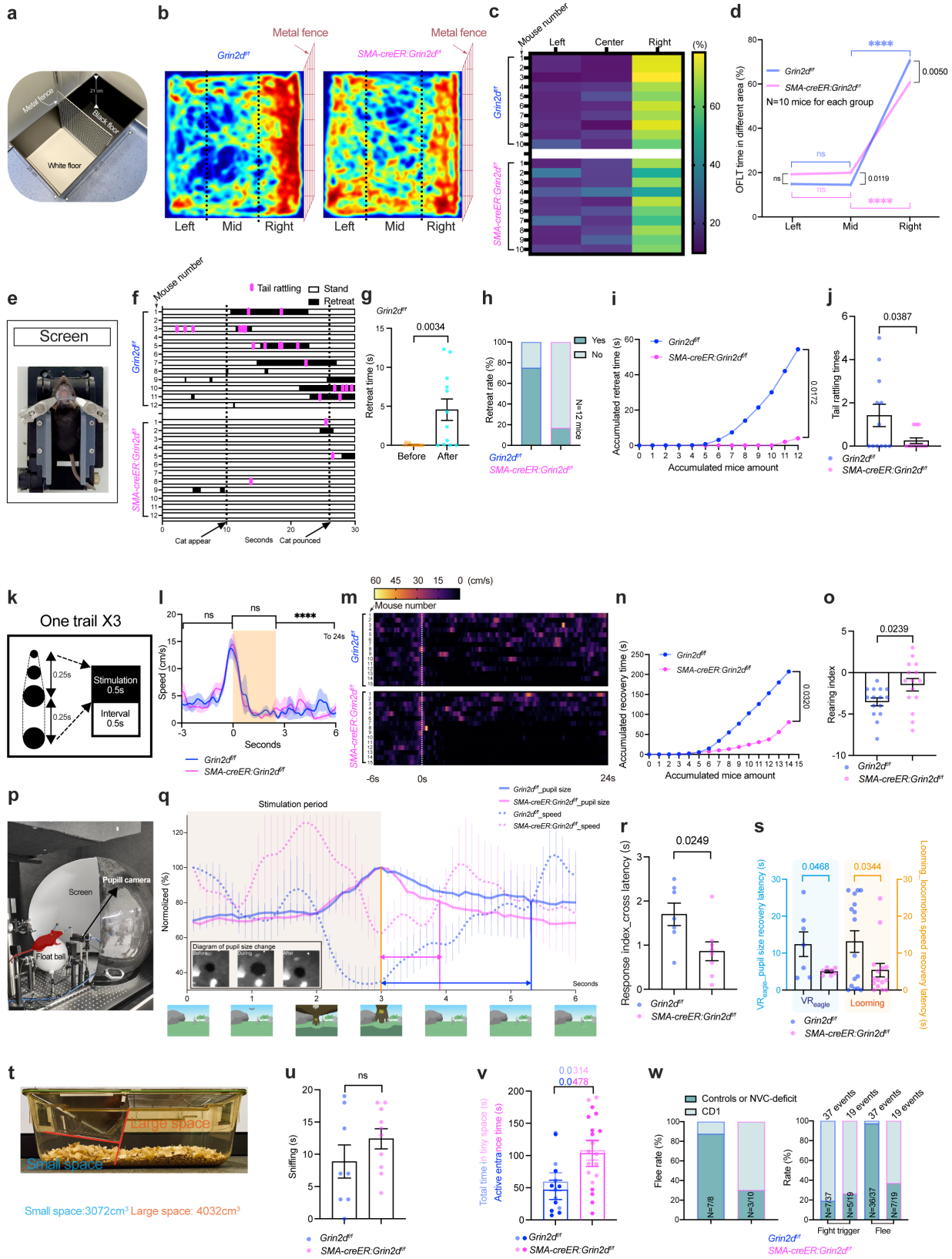

1191

1192 **Fig. 3 NVC is required to actively modulate the innate fear response. a,** The
1193 schematic diagram of the OFLT box setting. **b,** The schematic diagram of the trajectory
1194 heat map of *Grin2d*$^{f/f}$ and *SMA-creER:Grin2d*$^{f/f}$ mice in the OFLT. **c,** The heat map of mice
1195 stay rate in the left, middle, and right areas of the OFLT box. **d,** The statistical data for
1196 Figure 2c (n=10 mice for each group). **e,** The schematic diagram of Cat_{video} assay. **f,** The
1197 locomotion pattern of *Grin2d*$^{f/f}$ and *SMA-creER:Grin2d*$^{f/f}$ mice during the Cat_{video} assay. **g,**
1198 The retreat time of *Grin2d*$^{f/f}$ mice before and after cat appearance during the Cat_{video} assay.
1199 **h,** The retreat rate of *Grin2d*$^{f/f}$ and *SMA-creER:Grin2d*$^{f/f}$ in the Cat_{video} assay after cat
1200 appearance. **i,** The retreat time accumulation curve of *Grin2d*$^{f/f}$ and *SMA-creER:Grin2d*$^{f/f}$
1201 mice in the Cat_{video} assay after cat appearance. **j,** The tail rattling times of *Grin2d*$^{f/f}$ and
1202 *SMA-creER:Grin2d*$^{f/f}$ mice in the Cat_{video} assay after cat appearance. Raw data
1203 generating f-j panels shared the same bunch of mice (n=12 mice for each group). **k,** The
1204 schematic diagram of looming assay. **l,** The diagram of locomotion speed of *Grin2d*$^{f/f}$ and
1205 *SMA-creER:Grin2d*$^{f/f}$ mice from -3s to 6s in the looming assay. **m,** The locomotion speed
1206 heat map of *Grin2d*$^{f/f}$ and *SMA-creER:Grin2d*$^{f/f}$ mice from -6s to 24s in the looming assay.
1207 **n,** The subsiding status recovery latency accumulation curve of *Grin2d*$^{f/f}$ and *SMA-*
1208 *creER:Grin2d*$^{f/f}$ mice in the looming assay. **o,** The rearing index of *Grin2d*$^{f/f}$ and *SMA-*
1209 *creER:Grin2d*$^{f/f}$ mice in the looming assay. It is calculated by the rearing times after
1210 stimulation minus that before the stimulation. Raw data generating i-o panels shared the
1211 same bunch of mice (n=15 mice for each group). **p,** The exterior of the VR stimulation
1212 system. **q,** The normalized pupil size and locomotion speed of *Grin2d*$^{f/f}$ and *SMA-*
1213 *creER:Grin2d*$^{f/f}$ mice in the VR_{eagle} assay. **r,** The statistical data of response index from
1214 Figure. 3q. **s,** The statistical data of pupil size recovery latency and looming locomotion
1215 recovery latency from Figure. 3m and q. Raw data generating q-s panels shared the same

1216 bunch of mice (for VR_{eagle} assay, n=7 mice for each group, and for Looming assay, n=15
1217 mice for each group). **t,** The schematic diagram of CD1 social assay box setting. **u,** The
1218 sniffing times during the CD1 social assay. **v,** The total time of *Grin2d*$^{f/f}$ and *SMA-*
1219 *creER:Grin2d*$^{f/f}$ mice together with aggressive CD1 mouse in the small space (light color),
1220 and the time of *Grin2d*$^{f/f}$ and *SMA-creER:Grin2d*$^{f/f}$ mice in the small space when CD1 mice
1221 already stayed in the small space (deep color). **w,** The total flee rate of *Grin2d*$^{f/f}$ and *SMA-*
1222 *creER:Grin2d*$^{f/f}$ mice (counted as per mouse) after fight with aggressive CD1 mouse (left),
1223 and the normalized flee rate of *Grin2d*$^{f/f}$ and *SMA-creER:Grin2d*$^{f/f}$ mice (counted as per
1224 fight event) after fight with aggressive CD1 mouse (right). Raw data generating u-w
1225 panels shared the same bunch of mice (n=8 mice for *Grin2d*$^{f/f}$, and n=10 mice for *SMA-*
1226 *creER:Grin2d*$^{f/f}$). Data are presents as mean ± SEM.

Figure 4

Ruan et al.

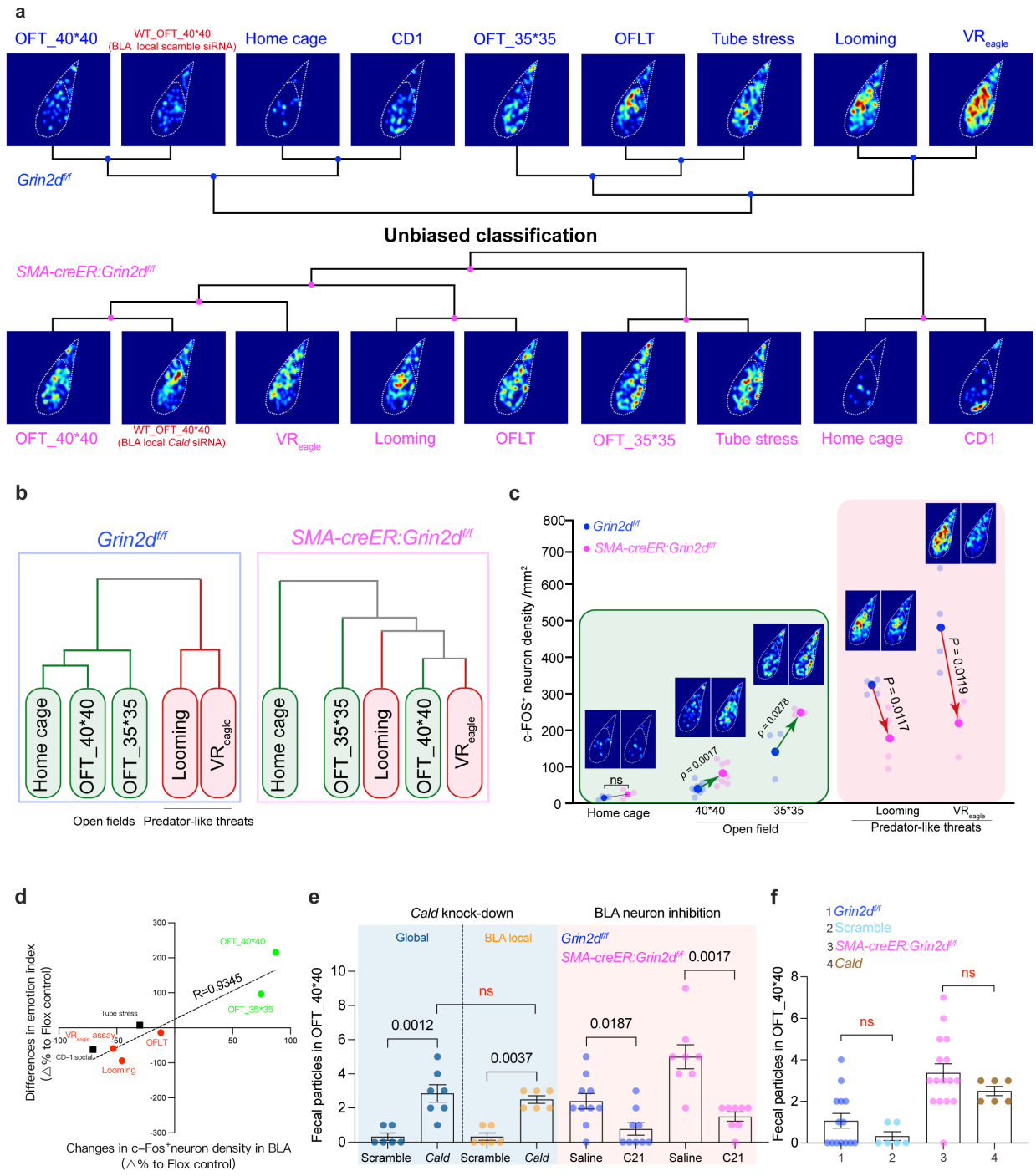

1227

1228

1229 **Fig. 4 NVC differentially regulates BLA neural activation. a,** Similarity index-based
1230 unbiased classification of c-Fos$^+$ neuron distribution pattern in BLA of the two genotypic
1231 lines across eight different contexts and BLA local siRNA interference in OFT_40*40. **b,**
1232 A similar classification as in a except for excluding tube stress, OFLT, and CD1 contexts.
1233 **c,** Quantification of the density of c-Fos $^+$ neurons in BLA under five contexts (n=4 for
1234 home cage, n=9 mice for OFT_40*40, n=4 mice for *Grin2d$^{f/f}$* in OFT_35*35, n=3 mice for
1235 *SMA-creER:Grin2d$^{f/f}$* in OFT_35*35, n=4 mice for each group in Looming and VR_{eagle}
1236 assay). **d,** Correlation between the level of BLA activation and the level of emotion indices.
1237 Hyper-response (higher emotion indices) mirrored with higher c-Fos$^+$ neuron density in
1238 BLA (green marks); Hypo-response (lower emotion indices) mirrored with lower c-Fos$^+$
1239 neuron density (red marks). For OFT_40*40, OFT_35*35, and tube stress (15 min), fecal
1240 production used for emotion index; for OFLT, time percentage in right area used for
1241 emotion index; for Looming assay, locomotion speed recovery latency used for emotion
1242 index; for VR_{eagle} assay, pupil size recovery latency used for emotion index; for CD1 social
1243 assay, time in small space used for emotion index. **e,** The fecal particles produced in
1244 OFT_40*40 by BLA global/local *Cald* knock-down mice (left 4 rows) and *Grin2d$^{f/f}$* and
1245 *SMA-creER:Grin2d$^{f/f}$* mice, respectively, after local BLA overexpression of hM4D (right 4
1246 rows). , n=6 mice for scramble siRNA group, n=6 mice for *Cald* siRNA group, n=10 mice
1247 for *Grin2d$^{f/f}$* saline group, n=9 mice for *Grin2d$^{f/f}$* C21 group, n=8 mice for *SMA-*
1248 *creER:Grin2d$^{f/f}$* saline group, and n=8 mice for *SMA-creER:Grin2d$^{f/f}$* C21 group. The raw
1249 data of cisternal magna siRNA injection (global) from Extended data Fig. 8i. **f,** The fecal
1250 particles produced in OFT_40*40 by BLA global/local *Cald* knock-down mice and *Grin2d$^{f/f}$*
1251 and *SMA-creER:Grin2d$^{f/f}$* mice, respectively. The raw data from Fig. 2c and Fig. 4e. Data
1252 are presents as mean ± SEM.

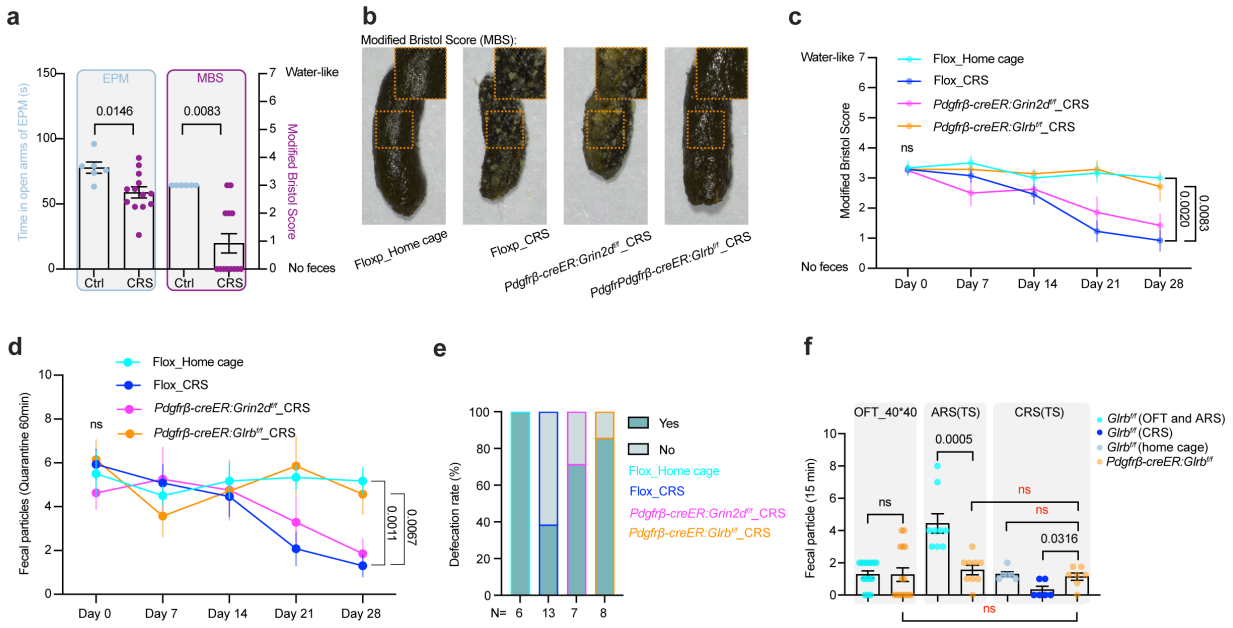

Fig. 5 The NVC-upregulation model showed emotional resistance to chronic restraint stress (CRS). a, The total time spent in open arms of EPM before/after the CRS and the Modified Bristol Score at day 28 of the CRS assay. **b,** Representative images of stools scoring of each group according to Modified Bristol Score assessment. **c & d**, Progressive changes in Modified Bristol scores and fecal particle number produced within a period of 60 min. The evaluation was performed before the assay and at the end of every week for consecutive 4 weeks of CRS. **e,** The defecation rate of each group. **f,** Profiling of differential defecation behavioral responses of the two genotypic lines across three contexts of OFT_40*40, acute restriction tube stress (ARS) and CRS. The raw data of OFT_40*40 and ARS from Figure 2c. Raw data generating a and c-f panels shared the same bunch of mice (n=6 mice for loxp_home cage, n=13 mice for loxp CRS groups, n=7 mice for *Pdgfrβ-creER:Grin2d*$^{f/f}$ and n=8 mice for *Pdgfrβ-creER:Glrb*$^{f/f}$ groups). Data are presents as mean ± SEM.